Title
HIGH TEMPERATURE FAILURE IN CERAMICS

Authors
Evans, A.G.
Blumenthal, W.

Publication Date
1981-07-01

Lawrence Berkeley Laboratory
UNIVERSITY OF CALIFORNIA

Materials & Molecular
Research Division

Presented at the International Symposium on Fracture Mechanics of Ceramics, Pennsylvania State University, University Park, PA, July 15-17, 1981

HIGH TEMPERATURE FAILURE IN CERAMICS

A.G. Evans and W. Blumenthal

July 1981

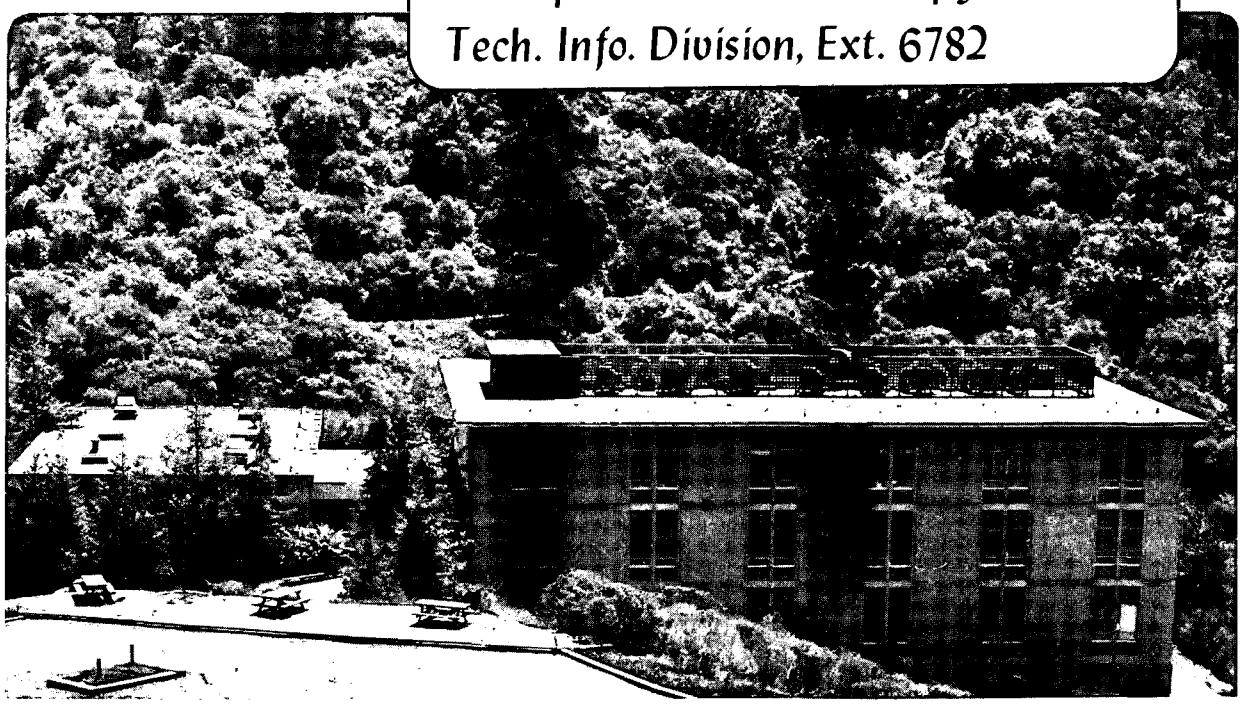

Prepared for the U.S. Department of Energy under Contract W-7405-ENG-48

DISCLAIMER

HIGH TEMPERATURE FAILURE IN CERAMICS

A. G. Evans and W. Blumenthal

Materials and Molecular Research Division, Lawrence Berkeley Laboratory
and Department of Materials Science and Mineral
Engineering, University of California
Berkeley, CA 94720

ABSTRACT

The failure of ceramics at elevated temperatures, accompanied by creep deformation, is substantially more complex than the brittle fracture process that prevails at lower temperatures. The failure typically involves a crack nucleation and a crack propagation stage. Both phenomena are associated with either diffusive cavitation or viscous hole growth. A framework suitable for the analysis and interpretation of the crack initiation and crack growth stages of failure is presented. Those aspects of the failure process that are relatively well comprehended are described in some detail, and current deficiencies in knowledge are emphasized.

This work was supported by the Director, Office of Energy Research, Office of Basic Energy Sciences, Materials Science Division of the U. S. Department of Energy under Contract No. W-7405-ENG-48.

1. INTRODUCTION

The mechanical failure of ceramics at elevated temperatures is accompanied by permanent deformation and consequently, exhibits a strong dependence on temperature and strain-rate (fig. 1). The failure usually evolves by the nucleation, growth and coalescence of cavities at preferred microstructural sites (fig. 1). The deduction of comprehensive engineering expressions for high temperature failure requires that the cavity evolution process be understood at the fundamental level. This paper describes the essential details that underlie the engineering analysis of failure.

High temperature failure typically involves two sequential processes: crack nucleation and crack propagation (fig. 2). Both processes must be comprehensively characterized in order to establish a generalized description of failure. The first part of the present paper is concerned with a characterization of crack propagation; while the second part is devoted primarily to cavitation mechanisms of crack nucleation. The implications for deriving engineering failure relations and for microstructural design are presented in the final section.

2. CRACK PROPAGATION

2.1 Morphological Observations

Observations of the crack tip region in materials subject to crack growth under creep conditions indicate the existence of a damage zone[1-3] (fig. 3). This damage zone consists of individual and coalesced cavities (a consequence of enhanced cavitation rates in the crack tip stress field). The crack advance under this circumstance appears to be incremental. Specifically, the crack tip remains stationary until the damage level

attains a sufficient intensity that the adjacent cavities merge with the crack. This constitutes a crack advance (fig. 4). The process then repeats, and a quasi-steady-state velocity results. The most intense damage is generally not coplanar with the crack (figs. 3,4) and consequently, the crack path is typically quite irregular[4] (relative to the more planar crack surfaces created during brittle fracture).

2.2 Crack Tip Fields

The characterization of crack extension-rates is determined by the parameter that dictates the amplitude of the singular field near the crack tip. For example, stress corrosion rates in elastic materials are adequately characterized by the stress intensity factor, K[5]. The situation is more complex under creep condtions[6]. The important singularity depends upon the manner in which the crack growth proceeds. For present purposes, it is required that the crack advance incrementally (section 2.1). Hence, immediately following a crack advance, the crack tip zone is subject to primary creep, characterized by

$$\dot{\varepsilon} = \dot{\varepsilon}_{op} \, (\sigma/\sigma_o)^{n_p} \, (\varepsilon/\varepsilon_{op})^{-m} \qquad (1)$$

where n_p and m are primary creep exponents and $\dot{\varepsilon}_{op}$, σ_o and ε_{op} are primary coefficients. The crack tip field under primary creep conditions is given by[6];

$$\sigma_{ij}/\sigma_o \propto [C_p(t)/r]^{(m+1)/(m+n_p+1)} \qquad (2)$$

where r is the distance from the crack tip and $C_p(t)$ is the stress field amplitude. If the primary creep field is embedded in an elastic field (a most likely situation following a crack increment), then;

$$C_p(t) = \frac{K^2(1-\nu^2)}{E}\left[\frac{m+1}{(m+n_p+1)t}\right]^{1/(m+1)} \tag{3}$$

where E is Young's modulus and ν is Poisson's ratio. The amplitude is thus expressible in terms of a time modified K[†]. Hence, if crack advance occurs while primary creep prevails at the crack tip and before the creep front advances to the specimen boundaries, the crack velocity should be adequately characterized by K.

For larger intervals following crack advance, the primary creep region will extend to the specimen boundaries and secondary creep will prevail at the crack tip,

$$\dot{\varepsilon} = \dot{\varepsilon}_{os}\,(\sigma/\sigma_o)^{n_s} \tag{4}$$

where n_s and $\dot{\varepsilon}_{os}$ are the secondary creep parameters. The crack tip field is then characterized by[6]

$$\sigma_{ij}/\sigma_o \propto [C_s(t)/r]^{1/(1+n_s)} \tag{5}$$

where

$$C_s(t) = \left[\frac{(n_s+m+1)C_p(t)}{(m+s)(n_s+1)}\right] t^{-m/(m+1)}$$

However, the far field is dictated by a primary creep region rather than an elastic region and K is thus an inadequate loading parameter. The crack growth behavior is best approximated by the asymptotic value of C_p[6];

$$C_p^* = \lambda a\,\sigma_\infty^{(m+n_p+1)/(m+1)} \tag{6}$$

[†]J would be more appropriate if the far field were subject to plastic deformation.

where σ_∞ is the applied stress, a is the crack length and λ is a proportionality constant that depends on the primary creep parameters and the far field loading.

Ultimately, for long crack advance waiting periods, as pertinent to low crack velocities, steady-state creep prevails throughout the specimen. The crack tip field is still characterized by eqn (5), but now C_s can be related to the applied loading by the time independent parameter[6];

$$C_s^* = F_s \sigma_s \dot{\varepsilon}_{os} a (\sigma_\infty/\sigma_o)^{1+n_s} \tag{7}$$

where F_s is a parameter that depends on the specimen geometry and loading.† Note that, for $n_s = 1$,

$$C_s^* \propto a \sigma_\infty^2 \equiv K^2/\pi \tag{8}$$

and the stress amplitude at the crack tip is uniquely determined by K. For typical practical ceramics, $1 \leqslant n_s \leqslant 2$; hence K should be a reasonable correlating parameter for most crack growth data. However, some non-uniqueness should be expected at low crack velocities, where C_s^* provides a more appropriate association between the crack tip field and the applied loading.

Finally, it is noted that, if the mechanism of crack advance involves the continuous motion of the crack tip, the amplitude of the crack tip field is dictated by the crack velocity[7]. Different crack growth characteristics are then likely.

2.3 Crack Growth Data

Most high temperature crack growth data have been evaluated using K as the appropriate loading parameter[8-10]. The uniqueness of K has been confirmed at high crack velocities[9], but its utility at low velocities has

†The equivalent parameter for elastic loading is, $F_E = K/\sigma\sqrt{\pi a}$

yet to be examined. Several interesting features emerge from the existent data.

The critical stress intensity factor for single phase materials, K_{IC}, decreases with increase in temperature[9], but can increase in materials that contain a continuous amorphous second phase at the grain boundaries[8-10]. The crack growth susceptibility increases as the temperature increases or as the viscosity of amorphous second phases decreases. Consequently, the exponent n_v that characterizes the crack velocity, v ,[10]

$$v/v_o = (K/K_{IC})^{n_v}$$

can exhibit a wide range of values (typically $6 < n_v < 10^3$), dependent upon temperature and composition. Adequate crack growth models must account for this range of possibilities.

Finally, it is noted that a threshold stress intensity K_{th}, for the growth of pre-existent cracks appears to exist[7,8](fig. 5). This threshold is manifest as a continuous crack opening without detectable growth (fig. 6). However, it should be recognized that, although pre-cracks appear to be stationary at K levels below the threshold, cracks can be generated elsewhere in the material[1] and initiate failure. Evidently, some complex nucleation/propagation behavior is involved below the threshold, which will require thorough investigation.

2.4 Crack Growth Models

Explicit crack growth models exist for cracks extending along the boundary between two grains by a process involving surface and grain boundary diffusion[11] (fig. 7). The analysis predicts that

$$K/K_G = 0.85\left[(v/v_{min})^{1/12} + (v/v_{min})^{-1/12}\right] \qquad (10)$$

where

$$K_G^2 = E(2\gamma_s - \gamma_b)(1-\nu^2)$$

$$v_{min} = 8(D_s\delta_s)^4\,\Omega\,[E/(1-\nu^2)D_b\delta_b]^3/kT\gamma_s^2$$

where γ_b and γ_s are the boundary and surface energies respectively, $D_s\delta_s$ and $D_b\delta_b$ are the surface and boundary diffusivities and Ω is the atomic volume. This relation anticipates a threshold K (fig. 7), as well as conforming with selected data[11]. However, the mechanism is not representative of the crack growth behavior in polycrystal aggregates; a process which involves incremental crack advance into a damage zone (section 2.1). An alternate, damage-zone, model is thus required (albeit that eqn (10) could describe the motion of individual cavities along grain boundaries within the damage zone).

A comprehensive damage zone model should incorporate the following features. The crack tip field in the absence of damage should be expressible in terms of K, C_p^* or C_s^*, depending upon the waiting period for crack advance. The damage should reduce the stress in the vicinity of the crack tip by virtue of constraint on the local volume expansion by the surrounding material. The damage should be in the form of grain boundary cavities activated by the normal stress; a requirement which would induce non-coplanar cavitation,† in accord with observation. Opening of the crack and coalescence with the cavities (to constitute a crack advance) should incorporate grain boundary sliding. Such a comprehensive model has not been developed. However, certain of the

†The maximum tension ahead of a crack occurs at an orientation $\theta \sim \pi/3$[12].

important requirements have been invoked in two recent attempts[6,13]. Bassani[6] has examined the growth of an individual coplanar activity within the various important singular fields. However, constraint effects have not yet been incorporated. Raj and Baik[13] have developed an essentially bi-crystal model with coplanar damage (fig. 8). The stress field amplitude is considered to be dictated by K and the growth of the damage is allowed to relax the stress near the crack tip. The crack is assumed to advance when the cavities coalesce with the crack tip. A threshold is also invoked, based on the threshold stress for cavity nucleation. Typical predictions are plotted in fig. 8. These models represent an important start, but clearly, much additonal refinement is required before a comprehensive model emerges.

3. CAVITATION MECHANISMS

3.1 Cavity Nucleation

Many ceramic materials prepared by sintering or hot pressing contain pre-existent cavities at grain boundaries; cavities which are not eliminated during final stage sintering. These cavities may exist at two, three or four grain junctions. Evidently, analysis of the evolution of cavities in such materials does not involve a nucleation requirement. In other ceramics, cavities are observed to initiate with time, following the application of stress. However, it is quite possible that the cavities nucleate immediately following the application of stress and then grow out to an observable size† with time, at variable rates. This situation is most

†Critical nucleation sizes ($\sim$10 - 100 Å) are below the resolution capability of most microscopic observation techniques.

plausible for nucleation at three or four grain junctions. For the latter, nucleation is spontaneous for dihedral angles $\Psi < 7\pi/18$; and occurs at modest stress levels for $\Psi \lesssim 5\pi/9$. Hence, cavities nucleate quite readily on grain boundaries with atypically small dihedral angles[14]. It will be demonstrated that cavity growth is also preferred on low Ψ boundaries and that cavitation prone boundaries frequently contain cavities with low measured values of Ψ. The dihedral angle (and its variability) is thus a central high temperature failure parameter.

Alternatively, cavities may be nucleated with time in the vicinity of three grain junctions or at grain boundary precipitates. Time-dependent nucleation can occur whenever grain boundary sliding transients exist (e.g. as the result of grain boundary rotation due to the glide and climb of intrinsic grain boundary dislocations). The transient introduces a peak tension[15] that can appreciably exceed the applied stress. The magnitude of the peak tension is dictated by the duration of the sliding transient (which establishes an elastic singularity) and the grain boundary diffusivity (which determines the stress redistribution rate). Explicit information concerning the viability of this nucleation mechanism does not yet exist.

For purposes of subsequent analysis, it is considered that sufficient cavities nucleate soon after stress application that the crack nucleation process is dominated by the propagation of the initially formed cavities (including their influence on enhanced nucleation and growth along adjacent boundaries).

3.2 Cavitation Origins

The cavitation process in polycrystalline materials is observed to be inhomogeneous[1,16,17]. Sites for preferred cavitation are of several types. In regions of uniform grain size (fig. 9) it will be demonstrated that cavities form preferentially on boundaries with a low Ψ or a low $D_s\delta_s$. Cavitation also occurs prematurely in zones of exceptional grain size (fig. 14), by virtue of an enhanced local stress. Finally, amorphous zones are susceptible to extensive cavitation because of a low local viscosity. The relative roles of these respective cavitation regions will be rationalized following the considerations of cavity growth (along grain boundaries) presented in the subsequent sections.

3.3 Constraints on Cavity Growth

The cavitation process in ceramic polycrystals is invariably observed to be inhomogeneous at the local level, as manifest in local cavity volume changes in excess of the average. The excess volume changes necessarily induce constraints which retard the cavitation rate and contribute importantly to the rupture time (fig. 10). The magnitude of the constraint is dictated by the viscous relaxation rate (associated with the surrounding material) relative to the rate of cavity volume change. Additionally, the constraint depends upon the morphology of the cavitation zone[18]. Two bounds are of practical import. For an isolated cavity, a maximum constraint $\hat{p}$ is experienced, given by[18];

$$\hat{p} = -4\eta_m \dot{e}^T \qquad (11)$$

where η_m is the viscosity of the surrounding material and $\dot{e}^T$ is the excess volume strain rate. For a coplanar array of cavities, a lower

bound constraint can be considered, such that the constraint p_η normal to the cavitation plane is given by[18];

$$p_\eta = -3\pi\eta_m\dot{\Delta\delta}/2d \qquad (12)$$

where $\dot{\Delta\delta}$ is the matter deposition rate between the individual cavities caused by excess cavity growth and d is the diameter of the cavitation zone (fig. 10). These constraints can be used to deduce the reduction in local stress acting upon the cavitation zone and thereby, to calculate cavity growth rates pertinent to typically observed inhomogeneous cavitation.

3.4 Constrained Cavity Propagation

3.4.1 Single Phase Materials

Cavities in fine-grained single phase materials typically nucleate at three grain junctions and extend across grain facets that lie approximately normal to the applied tension. The growth process occurs in three principle stages[18] (fig. 11): the uniform expansion of equilibrium cavities (cavities with a uniform surface curvature), the preferred growth of crack-like cavities and the thickening of full-facet cavities. Isolated equilibrium cavities (fig. 11a) move at a constrained velocity[18]

$$\frac{\dot{a}_{eqn}kT\ell^3}{\Omega D_b\delta_b\gamma_s} = \left(\frac{14\pi}{3}\right)\frac{[(3/4)(\sigma_\infty\ell/\gamma_s)f - (4\sqrt{3})h(\Psi)(1-f)]}{F(\Psi)f^2} \qquad (13)$$

where ℓ is the grain facet length, f is the relative cavity length (a/ℓ), σ_∞ is the applied stress, $h(\Psi) = \sin(\pi/2-\pi/6)$ and

$$F(\Psi) = 1 + \frac{\sqrt{3}[\Psi-\pi/3 - \sin(\Psi-\pi/3)]}{2\sin^2(\Psi/2 - \pi/6)} \qquad (14)$$

The velocity trend is depicted schematically in fig. 12 as a function of the important variables. The equivalent result for the crack-like cavity (fig. 11b) is[8]

$$\frac{\dot{a}_{crack} kT\ell^3}{\Omega D_b \delta_b \gamma_s} \approx \left(\frac{0.15\sigma_\infty \ell}{\gamma_s \sin(\Psi/4)\Delta^{1/3}} \right)^{3/2} \tag{15}$$

where $\Delta = D_s\delta_s/D_b\delta_b$. The cavity velocities are plotted in fig. 12.

The time taken for cavities to extend across the grain facet can be determined from eqns (13) and (15) as plotted in fig. 13. The propagation time is typically dominated by the constrained crack-like growth. This feature may be used to deduce an approximate propagation time[18];†

$$t_p \dot{\varepsilon}_\infty \approx \frac{50\,\pi \sin^{3/2}(\Psi/4)\Delta^{1/2}}{(\sigma_\infty \ell/\gamma_s)^{1/2}} \tag{16}$$

Once a full-facet cavity has formed, its extension along the neighboring grain boundaries is restricted by the existence of the two impinging grain boundaries. Specifically, extension along one or both of these boundaries would require the development of appreciable negative surface curvatures, which are only tenable for small values of Δ. Consequently, full-facet cavities expand primarily by a thickening process (fig. 11c). The constrained rate of thickening $\dot{y}$ for an isolated full-facet cavity is given by[17];

$$\frac{\dot{y} kT\ell^3}{D_b \delta_b \Omega \gamma_s} = \frac{12\sigma_\infty \ell/\gamma_s}{[1 + 2/\Delta + 12\sqrt{3}/7\pi]} \tag{17}$$

---

†The influence of the grain boundary diffusivity on t_p is implicitly contained in $\dot{\varepsilon}_\infty$, which is $\propto D_b\delta_b$.

In coarse grained ceramics, cavitation is observed to occur predominantly on two grain boundaries (fig. 14). The cavity nuclei probably pre-exist as residual sintering cavities, but cavities may also nucleate at grain boundary precipitates. The trends in cavity velocity are essentially the same as those described above for the triple junction cavities. Explicit results can be located in the papers by Chuang et al.[19], and by Rice[20].

3.4.2 Two Phase Materials

Materials prepared by liquid phase sintering, which usually contain a continuous amorphous phase around the grains, exhibit unique cavitation characteristics. The cavitation can occur by hole growth within the amorphous phase and/or by solution/reprecipitation. Again, the cavitation appears to occur primarily at three grain junctions in regions of small grain facet length (fig. 15)[21].

Viscous hole growth along the boundary between two grains has been analyzed by Raj and Dang[22] and by Evans[23]. These analyses demonstrate that the time required to create a facet-sized cavity under constrained conditions is given by;

$$t_p \dot{\varepsilon}_\infty = \lambda (b/\delta_0)^2 \qquad (18)$$

where b is the spacing between cavities, δ_0 the initial thickness of the amorphous phase, and the coefficient λ depends primarily on the grain size and the viscosity of the fluid.

The growth rate of holes located within amorphous pockets at three grain junctions also depends on the viscosity and initial thickness of the amorphous material. The parameter of initial significance is the time

taken to deplete the pocket of amorphous material, t_c . This time under constrained conditions is given by[23];†

$$t_c \dot{\varepsilon}_\infty \approx \frac{4}{3}\left(\frac{\delta^3}{\delta_o^2 \ell}\right) \frac{(1-a/\ell)}{[1 - 3(a/\ell) + 3(a/\ell)^2 - (a/\ell)^3]} \tag{19}$$

where a is the pocket size and δ is the channel thickness at pocket depletion. Subsequent to depletion, the cavities extend within the channel, either by means of multiple hole growth[22,23] or by the formation of finger-like entities[24].

Finally, it is noted that, with very thin amorphous films and planar facets, a grain boundary sliding and brittle cracking process can occur. This process is characterized by the appearance of facet-sized cracks at a time, t_p . The propagation time is dictated by coupled crack growth and elastic relaxation of the sliding boundary, such that[25],

$$t_p = \frac{2\gamma_{g.b.}\eta_b}{\sigma_\infty^2 \delta_o} \tag{20}$$

where $\gamma_{g.b.}$ is the grain boundary fracture energy and η_b is the boundary viscosity. This process in not constrained by the surrounding material and hence, there is no explicit influence of the steady state creep on the propagation time.

4. CRACK NUCLEATION: CAVITY COALESCENCE

The final stage of crack nucleation concerns the coalescence of sufficient contiguous cavities that a discrete crack can be considered to exist. This coalescence process takes several forms, depending upon the nature of the individual cavity propagation events. Two primary modes

†The viscosity η of the amorphous liquid is implicit in $\dot{\varepsilon}_\infty$ ($\dot{\varepsilon}_\infty \propto \eta$).

of coalescence have been considered; a high stress mechanism in which each cavity is treated as an independent entity, and a low stress mechanism dominated by cavity interaction effects. Both processes will be briefly examined in the subsequent section.

4.1 Non-Interactive Coalescence

When the stress is relatively large, most of the cavitation processes discussed in section 3.4 result in narrow (e.g. crack-like) cavities. The matter displaced in cavity formation is thus relatively small and can, in many instances, be accommodated by partial release of the elastic strain in the adjacent grains, by means of a grain boundary sliding process[26] (fig. 16). In consequence, the tensile stress enhancement on the neighboring grain boundaries is relatively small and the cavitation at individual grain boundaries can be regarded as approximately non-interactive. Crack nucleation can then be treated using a probabilistic approach, characterized by the probability that there be a sufficient number of contiguous narrow cavities to comprise a discrete macrocrack. For this purpose an identifiable macrocrack is assumed to exist when the stress intensity attains some fraction ξ of the critical stress intensity factor, K_c (e.g. $\xi K_c = K_{th}$). A probabilistic treatment of contiguity, by specifying independence of the individual cavity formation probabilities, yields the following result[26];

$$\ell n[t_n \exp(Q/RT)] = A - n\ell n\sigma_\infty - \sigma_\infty^2(4\ell/\pi k\xi^2 K_c^2)\ell n(4A_T/\ell^2) \qquad (21)$$

where t_n is the nucleation time, Q is the activation energy for the cavity propagation process, A_T is the total grain boundary area, k is the shape parameter that characterizes the statistical variability of the

cavitation process on individual grain boundaries ($1 < k < 10$). A and n are constants that depend on the mechanism of cavity propagation; for example, cavitation involving the viscous flow of an amorphous phase gives[26];

$$\eta = 1$$
$$A = 0.3\eta(\ell/\delta_o)^2 \qquad (22)$$

The quantity, $t_n \exp(Q/RT)$, has been termed the Orr-Sherby-Dorn parameter; a parameter which correlates failure data over a wide range of test conditions (given that the same mechanism dictates failure).

This analysis conforms quite well with relatively high stress time-to-failure data obtained on fibers of SiC and Al_2O_3 (fig. 17). It may also provide an approximate description of time dependent crack nucleation in other material systems at intermediate temperatures.

4.2 Zone Spreading

The cavities that develop at lower stress levels are of sufficient width that isolated cavities are subject to appreciable constraint from the surrounding material (section 3.3). This constraint results in the development of enhanced tensions at the perimeter of the cavitation zone (fig. 10d). This enhanced tension can accelerate cavity propagation, as well as nucleating additional cavities in the peripheral zone. When the cavity size in the peripheral zone becomes equal to that in the cavitation zone, an enlarged cavitation zone results. The cavitation process then extends into a new peripheral zone (fig. 18). This process has been referred to as zone spreading[18].

Zone spreading considerations are based on the premise that initial cavity development on certain boundaries is associated with a small local dihedral angle (section 3.4) or a low local viscosity. The resultant zone spreading process can then be conveniently separated into three regimes. Firstly, when the deviations Ψ or η are small, and the absolute values are close to the average for the material, zone spreading occurs very rapidly, while the cavities are still quite small (fig. 19a). Failure from these regions is expected to occur quite slowly, at a rate similar to that for a homogeneous material. This regime is of the least practical significance, because failure initiates in regions of more substantial inhomogeneity. Conversely, when there are appreciable local deviations in Ψ or η, a cavity can extend fully across a grain facet before significant cavitation can be induced on the contiguous boundaries (fig. 19b). The cavitation can then by regarded as an essentially independent process. This cavitation regime is likely to pertain in isolated regions† during the early stages of failure, and explains the observation of premature full-facet sized cavities[17]. If a relatively large proportion of boundaries exhibit high cavitation susceptibility, premature failure may occur from continuous accumulations of these boundaries. The probabilistic aspects of failure under these conditions are similar to those described in the preceding section (3.5.1).

Finally, an intermediate regime exists, wherein cooperative cavity coalescence encourages relatively rapid crack initiation (fig. 19c). Such regions are thus regarded as principal sites for crack initiation in the

†The number of these regions would be dictated by the probability of locating a boundary with small values of Ψ based upon the appropriate statistical distribution.

absence of statistical accumulations of high susceptibility boundaries. The trends in cavity propagation during zone spreading suggest that an appreciable proportion of the crack nucleation time in the intermediate region is consumed while the cavity is contained along one or two grain facets[18]. The approximate expression for the cavitation time (eqn 16) that pertains during this period should thus provide a first-order estimate of crack nucleation. The quantity $t_p\dot{\varepsilon}_\infty$ should then be replaced by $t_n\dot{\varepsilon}_\infty$: the Monkman-Grant parameter. This parameter has been observed to correlate a wide range of creep rupture data on metallic systems.

4.3 Premature Crack Nucleation

There are several important sources of premature high temperature crack nucleation in ceramics (section 2.2); notably isolated amorphous regions in otherwise single phase material and zones of exceptional grain size[27]. The latter appears to be of particular importance (fig. 20) and hence, the evolution of premature nucleation from large grained zones is emphasized in this section.

A large grained region in a solid subject to creep deformation has a higher visocsity than the matrix, because of the strong grain size dependence of the creep rate (either Herring-Nabarro or Coble creep). This region must therefore experience stresses in excess of the applied stress (fig. 20). This enhanced tension can accelerate the cavity propagation process and thus prematurely initiate a crack. However, it is also important to recognize that a fully cavitated large grained zone may not represent a discrete microcrack, because the resultant K associated with the crack nucleus may be less than the threshold level, K_{th} , for crack propagation (section 2.3). Studies concerned with these issues are in progress.

5. IMPLICATIONS AND CONCLUSIONS

The observations and analysis of high temperature cavitation summarized in the present paper indicate the inhomogeneous nature of high temperature failure in ceramics. A frequent consequence of the inhomogeneity (and the resultant development of constraint) is the inverse dependence of the failure time on the steady-state creep rate of the material (Monkman-Grant behavior). Within this regime, any microstructural modification that reduces the creep rate should thus produce a proportional increase in the failure time. This correlation provides an invaluable basis for the design of failure resistant microstructures.

Monkman-Grant behavior may be violated under certain conditions; notably at intermediate temperatures and high stresses, or in the presence of a high proportion of cavitation susceptible boundaries. Constraint effects are then minimal and failure is based on the statistical accumulation of contiguous cavities. A probabilistic analysis of this process indicates that failure in this instance is governed by an Orr-Sherby-Dorn parameter, such that the activation energy term in the parameter is related to that for the dominant cavitation process.

The failure times in both the Monkman-Grant and Orr-Sherby-Dorn regimes are also predicted to depend on other material properties. In single phase materials, low values of the dihedral angle and of surface diffusivity are found to be deleterious. Low dihedral angles (high grain boundary energies) may be inevitable in ceramics (by virtue of covalent or ionic bonding characteristics). However, there may be important influences (both beneficial and deleterious) of solutes, which merit further study. A low surface diffusivity may also be inevitable for typical ceramics, as required for the initial

stage sintering[28]. But again, explorations of the temperature dependence of the diffusivity and of solute effects may indicate situations which retard cavitation without detracting from the sinterability.

In two phase materials with a continuous second phase, the important material variables are the thickness of the second phase and its viscosity. Large values for the thickness and low viscosities encourage rupture, as might be intuitively expected. Chemical control is thus a central concern for the creep rupture of these materials.

It has also been demonstrated that several important sources of premature failure can exist in typical ceramics†: in particular, large grained zones and zones of amorphous material in otherwise single phase materials. Premature failure results from the development of either large local stresses (large grained zones) or from regions of high cavitation susceptibility (amorphous zones). The elimination of large scale heterogeneities is thus an essential requirement for the prevention of premature failure[16].

The preceding behavior refers to crack nucleation controlled creep rupture, as expected for long lifetimes, particularly at elevated temperatures. The conditions that cause failure to be dominated by crack nucleation, rather than crack propagation, are still rather nebulous; although, observations of crack propagation thresholds begin to suggest effects which distinguish nucleation control from propagation control.

When crack growth controls failure (as might be expected, for example, in the presence of surface cracks subject to stress intensity levels in excess of the threshold), the loading parameter used to describe the crack growth rate should be chosen carefully. At low crack velocity, C_s^*, is

†It is notable that these heterogeneities differ in character from those that typically dictate the brittle fracture process at lower temperatures[16].

the appropriate choice. However, C_s^* and K are essentially equivalent for linearly viscous materials and hence, K may be an adequate loading parameter for most ceramics (which exhibit creep exponents between 1 and 2).

ACKNOWLEDGMENT

This work was supported by the Director, Office of Energy Research, Office of Basic Energy Sciences, Materials Science Division of the U.S. Department of Energy under Contract No. W-7405-ENG-48.

REFERENCES

1. W. Blumenthal and A. G. Evans, to be published.
2. N. J. Tighe, Jnl. Mat. Sci. 13 (1978) 1455.
3. D. R. Clarke, to be published.
4. K. R. Kinsman, R. K. Govila and P. Beardmore, Deformation of Ceramic Materials (Ed. R. C. Bradt and R. E. Tressler), Plenum, N. Y. (1974) p. 465.
5. S. M. Wiederhorn, Fracture Mechanics of Ceramics (Ed. R. C. Bradt, F. F. Lange and D. P. H. Hasselman) Plenum, N.Y. (1974), vol. 2, p. 613.
6. J. L. Bassani, Creep and Fracture of Engineering Materials and Structures (Ed. B. Wilshire and D. R. J. Owen), Pineridge, Swansea, U.K. (1981) p. 329.
7. H. Hiu and H. Riedel, Intl. Jnl. Frac. 16 (1980).
8. M. H. Lewis, B. S. B. Karunaratne, J. Meredith and C. Pickering, Creep and Fracture of Engineering Materials and Structures, ibid., p. 365.
9. A. G. Evans, L. E. Russell and D. W. Richerson, Met Trans. 6A (1975) 707.
10. A. G. Evans and S. M. Wiederhorn, Jnl. Matls. Sci. 9 (1974) p. 270.
11. T. J. Chuang, Jnl. Amer. Ceram. Soc., in press.
12. A. G. Evans, A. H. Heuer and D. L. Porter, Fracture 77 (Ed. D. M. R. Taplin) Univ. Waterloo Press, Waterloo 1977 (vol. 1) p. 520.
13. R. Raj and S. Baik, Metal. Science 14 (1980) p. 385.
14. R. M. Cannon, to be published.
15. A. G. Evans, J. R. Rice and J. P. Hirth, Jnl. Amer. Ceram. Soc. 63 (1980) p. 368.

16. A. G. Evans, Jnl. Amer. Ceram. Soc., in press.

17. J. R. Porter, W. Blumenthal and A. G. Evans, Acta Met., in press.

18. C. H. Hsueh and A. G. Evans, Acta Met., in press.

19. T. J. Chuang, K. I. Kagawa, J. R. Rice and L. B. Sills, Acta Met. 27 (1979) 265.

20. J. R. Rice, Acta Met. 29 (1981) p. 675.

21. F. F. Lange, R. I. Davis and D. R. Clarke, Jnl. Mater. Sci. 15 (1980) 601.

22. R. Raj and C. H. Dang, Phil. Mag. 32 (1975) 909.

23. A. G. Evans, to be published.

24. R. J. Fields and M. F. Ashby, Phil. Mag. 33 (1976) 33.

25. A. G. Evans, Acta Met. 28 (1980)1155.

26. A. G. Evans and A. Rana, Acta Met. 28 (1980).

27. S. Johnson, W. Blumenthal and A. G. Evans, to be published.

28. M. F. Ashby, Acta Met. 22 (1974) 275.

FIGURE CAPTIONS

Fig. 1 A schematic indicating the temperature dependence of the strength of a typical ceramic.

Fig. 2. A schematic indicating that the failure time at elevated temperatures typically includes a crack nucleation and a crack propagation stage.

Fig. 3. A crack tip damage zone in Al_2O_3 tested at 1450°C to a strain of 0.027 at a stress intensity level of $1.85MNm^{-3/2}$ ($K_c = 2.27MNm^{-3/2}$)

Fig. 4. A schematic indicating the crack advance sequence in the presence of a damage zone.

Fig. 5. Crack growth rate data for various silicon nitrides indicating the existence of a threshold.

Fig. 6. The opening of a pre-existent crack in Al_2O_3 at stress intensities below the threshold.

Fig. 7. A schematic showing the crack growth along the boundary by a process involving surface and boundary diffusion and the resultant stress intensity, cavity velocity diagram.

Fig. 8. A schematic indicating the coplanar bicrystal damage model of Raj and Baik[13], and the resultant cavity growth predictions.

Fig. 9. Cavitation in a region of uniform grain structures.

Fig. 10. A schematic indicating the development of constraint due to inhomogeneous cavitation within a cavitation zone.

Fig. 11. The three stages associated with the growth of individual cavities: (a) equilibrium, (b) crack-like and (c) full-facet.

Fig. 12. The velocity of equilibrium and crack-like cavities as a function of the important variables[18].

Fig. 13. Cavity propagation times derived from fig. 12.[18]

Fig. 14. Cavitation in a coarse grained region of an Al_2O_3 specimen occurring on boundaries between two grains[27].

Fig. 15. Cavitation in Si_3N_4 indicating hole formation between grains in a large grained region and at three grain junctions in a fine grained region[21].

Fig. 16. The accommodation of narrow cavities by grain boundary sliding and elastic relaxation.

Fig. 17. A comparison of measured failure times for (a) Al_2O_3 and (b) SiC fibers with predictions based on a probabilistic analysis assuming statistically independent cavity growth processes.

Fig. 18. A schematic illustrating the zone spreading process.

Fig. 19. The growth times of cavities in the cavitation and peripheral zones (a) rapid spreading, (b) full-facet cavity formation and (c) intermediate spreading.

Fig. 20. A large grained failure origin in an Al_2O_3 material tested at elevated temperatures, and the stress concentration that develops in this region.

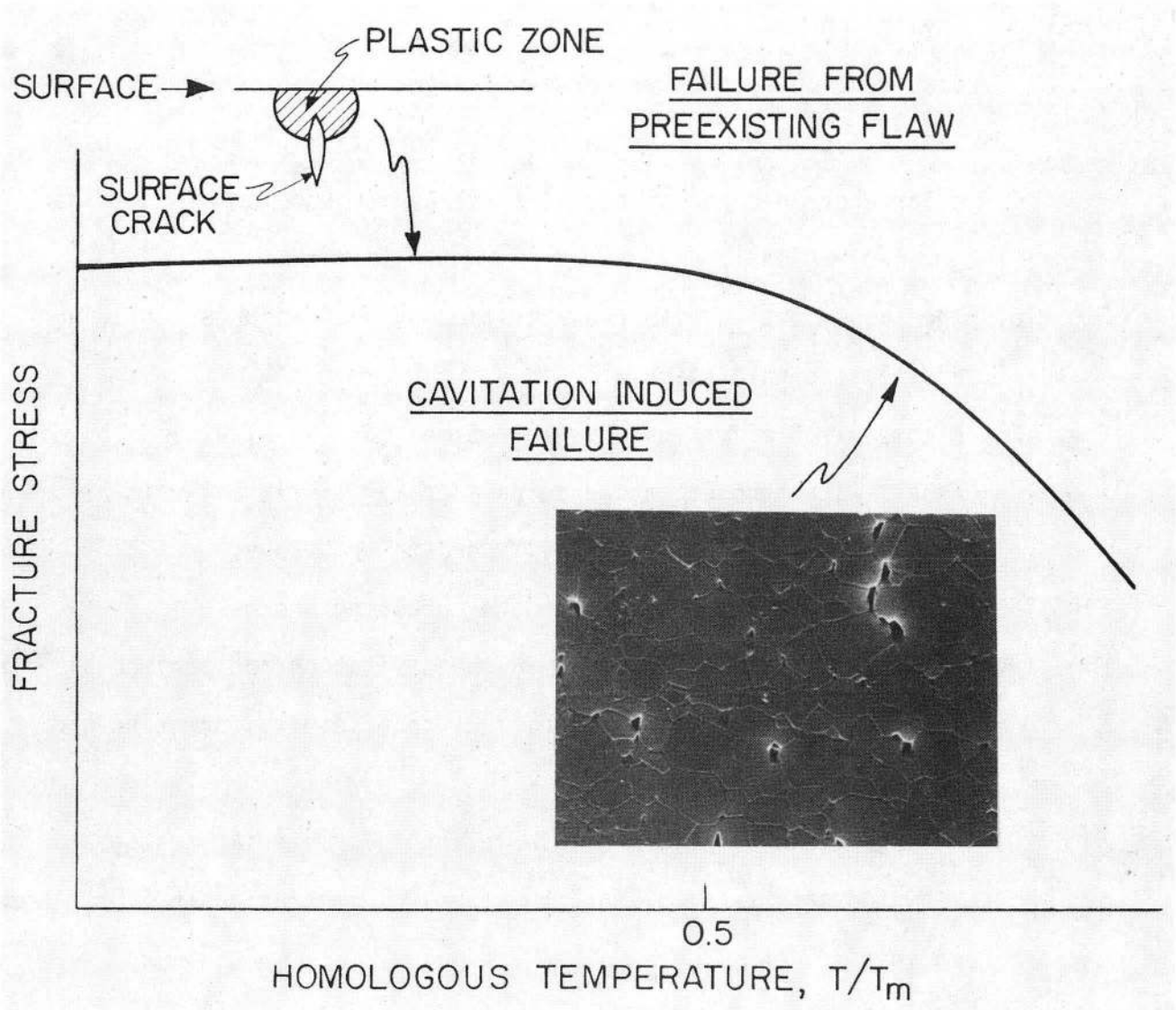

XBB813-2479

Fig. 1

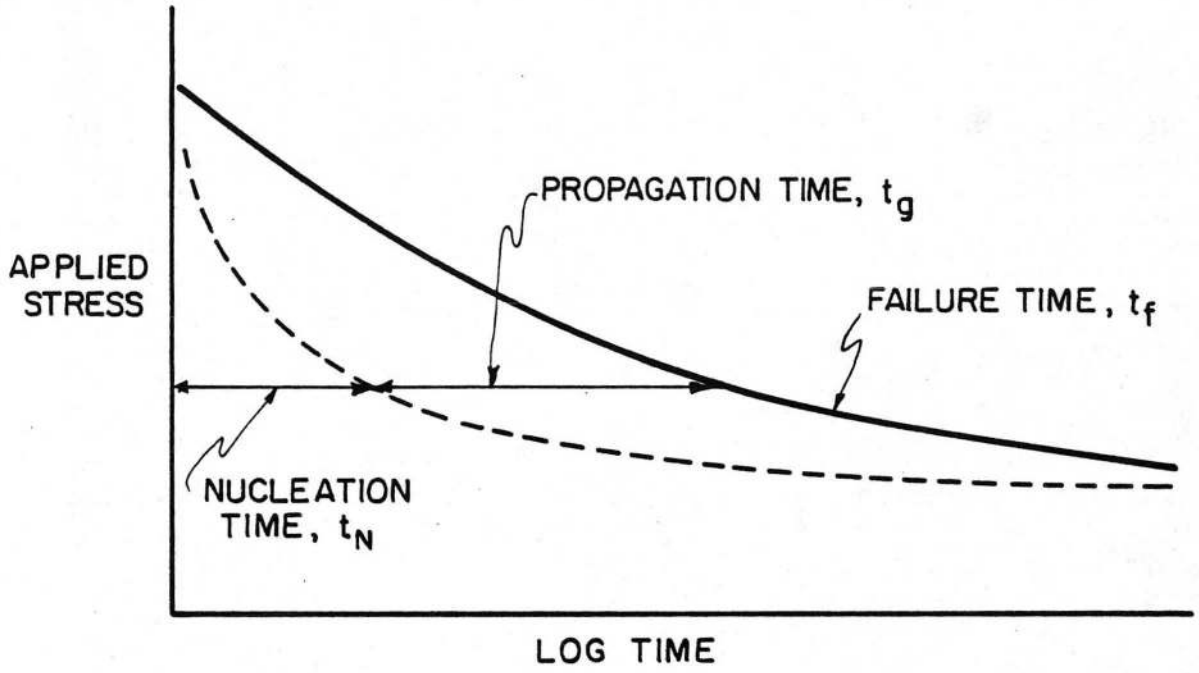

XBL816-6007

Fig. 2

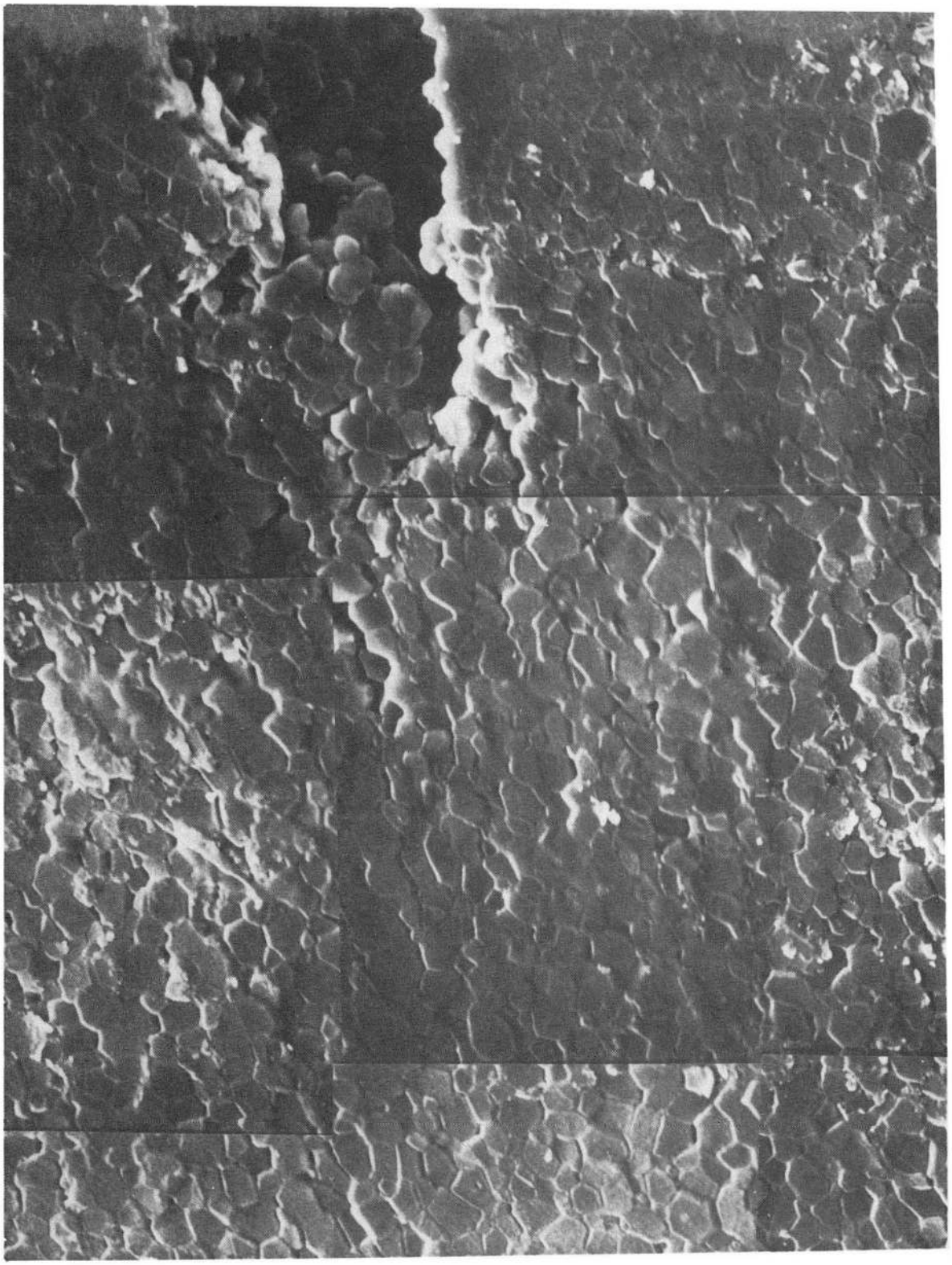

XBB817-6185

Fig. 3

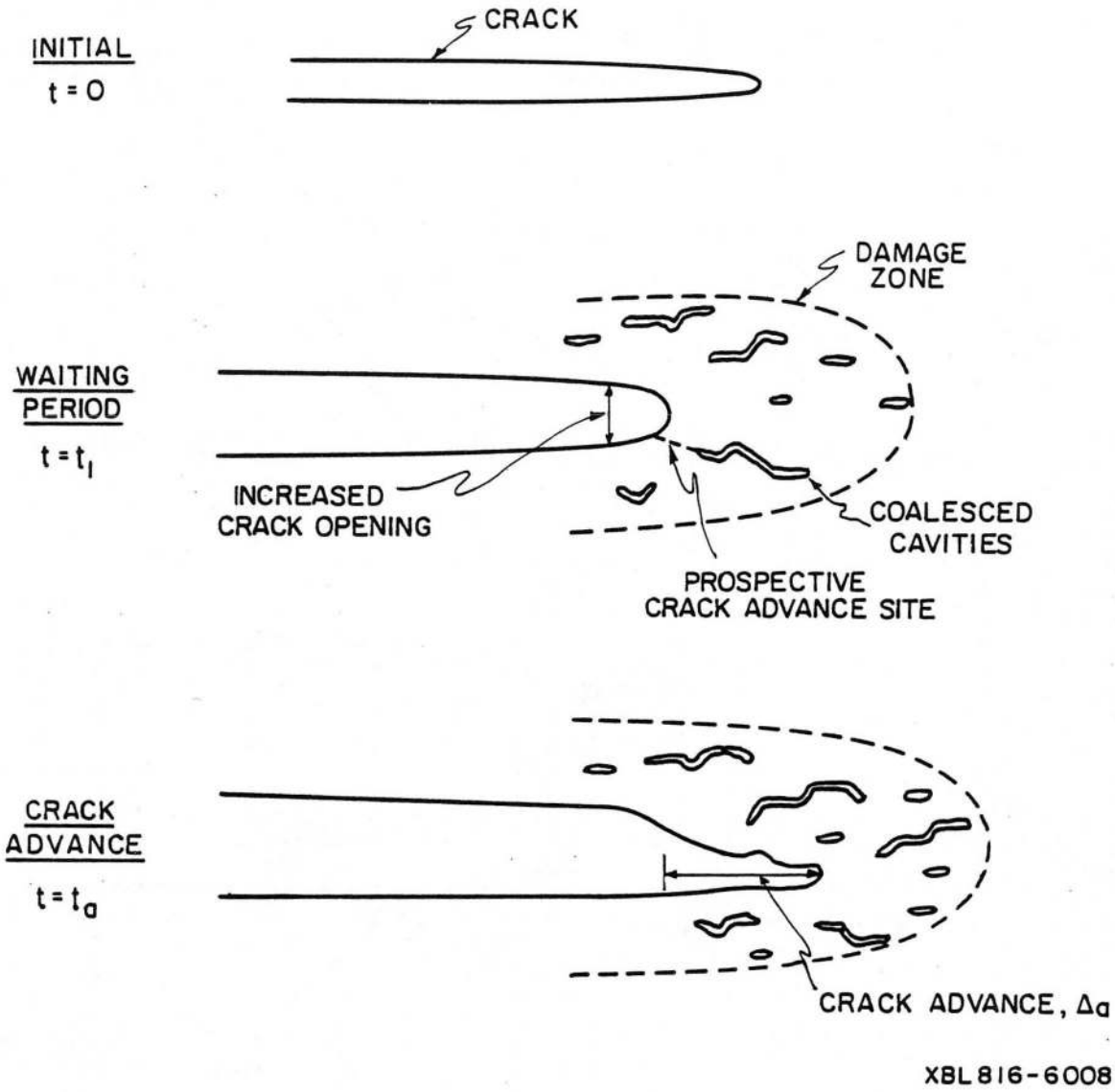
INITIAL
t = 0
CRACK
WAITING PERIOD
t = t_I
DAMAGE ZONE
INCREASED CRACK OPENING
COALESCED CAVITIES
PROSPECTIVE CRACK ADVANCE SITE
CRACK ADVANCE
t = t_a
CRACK ADVANCE, Δa
XBL 816-6008

Fig. 4

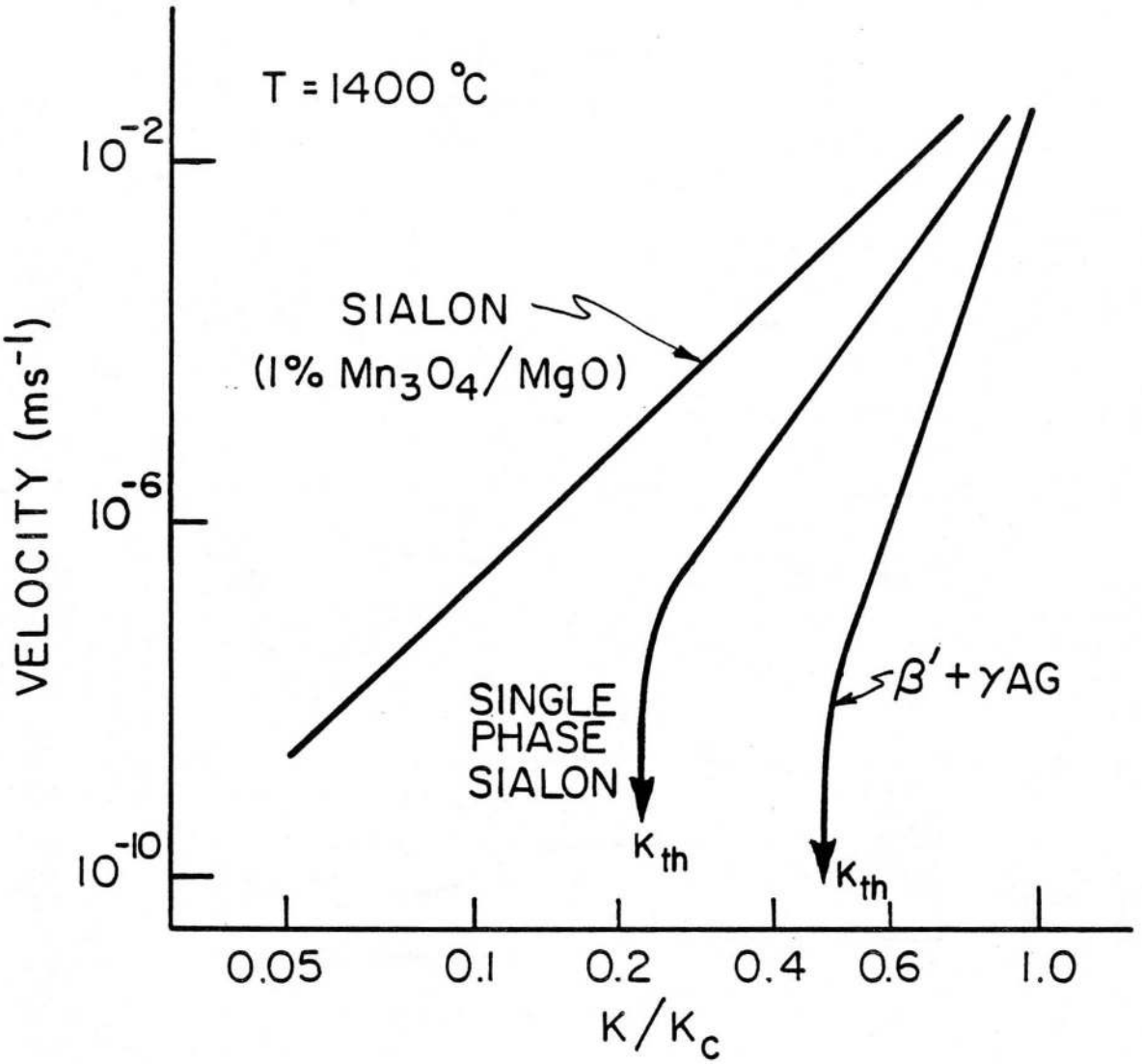

XBL 816-6003

Fig. 5

XBB817-6365

Fig. 6

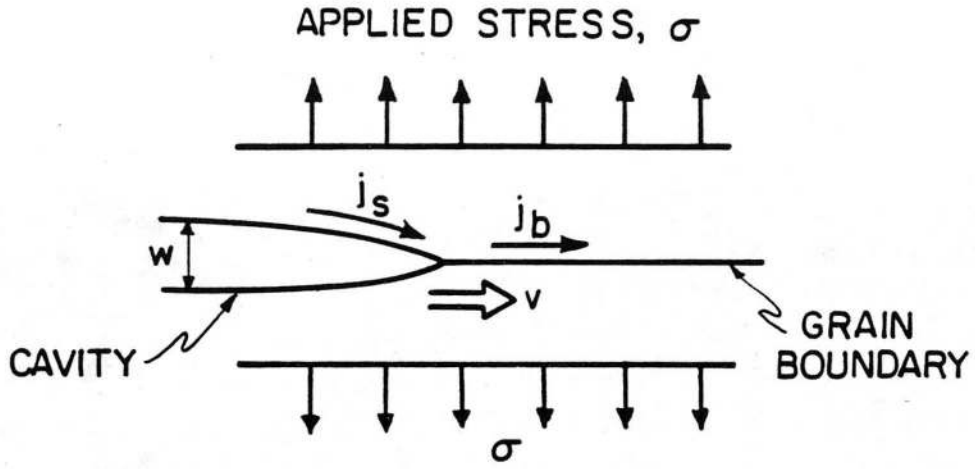
APPLIED STRESS, σ
j_s
j_b
w
v
CAVITY
GRAIN BOUNDARY
σ

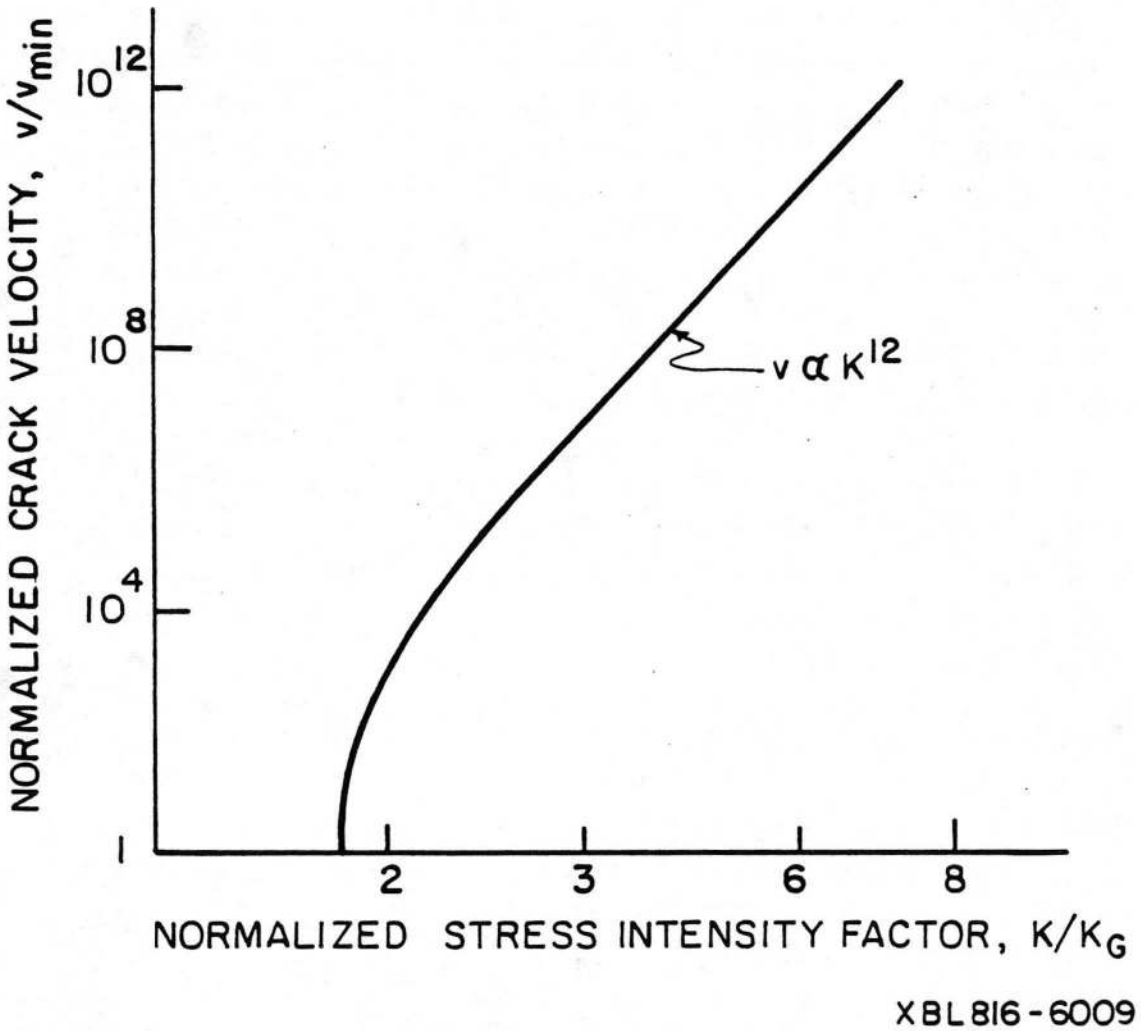
NORMALIZED CRACK VELOCITY, v/v_{min}
10^{12}
10^{8}
10^{4}
1
$v \propto K^{12}$
2
3
6
8
NORMALIZED STRESS INTENSITY FACTOR, K/K_G
XBL816-6009

Fig. 7

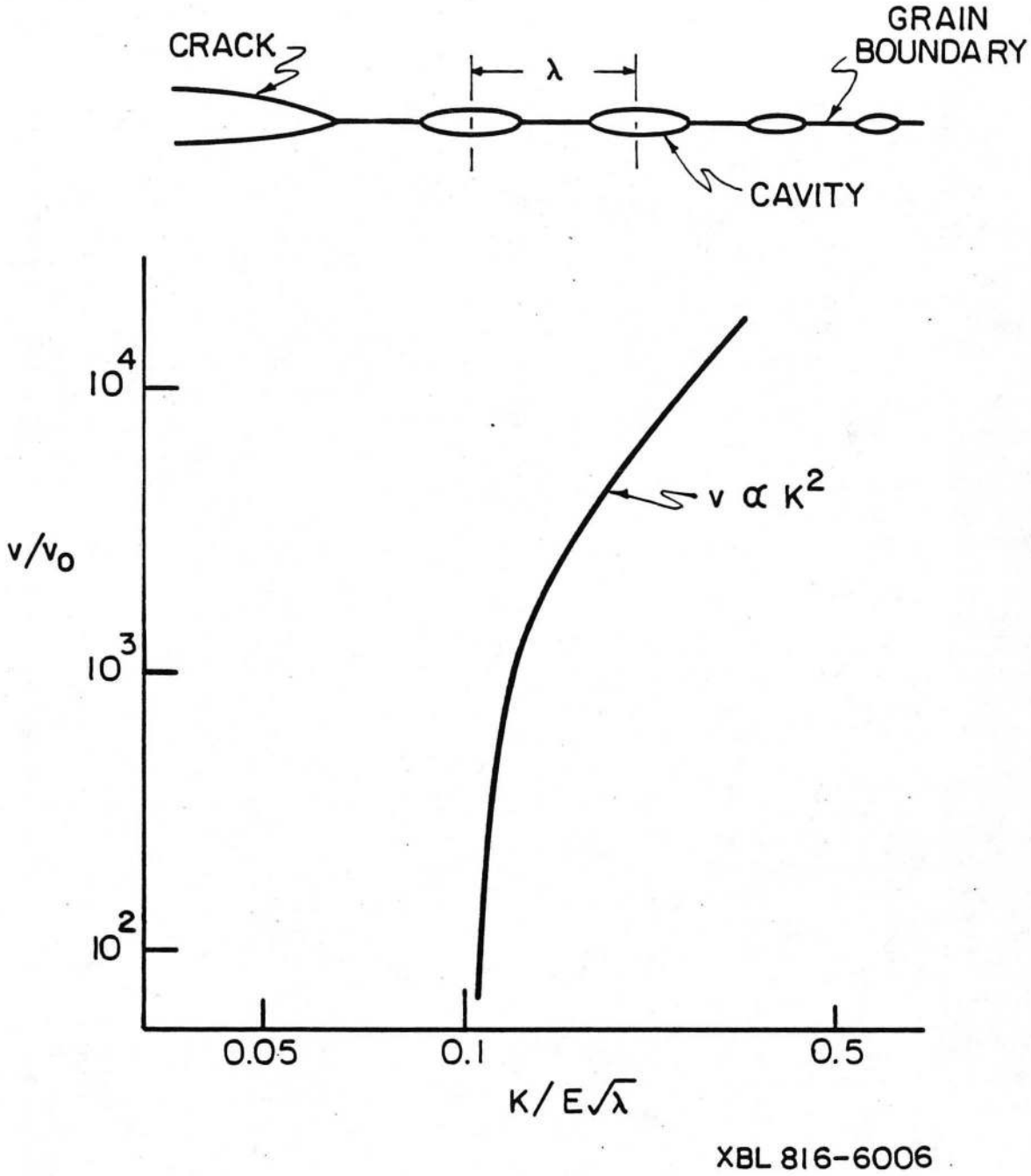
CRACK
λ
GRAIN BOUNDARY
CAVITY
10^4
10^3
10^2
v/v_o
$v \propto K^2$
0.05
0.1
0.5
$K/E\sqrt{\lambda}$
XBL 816-6006

Fig. 8

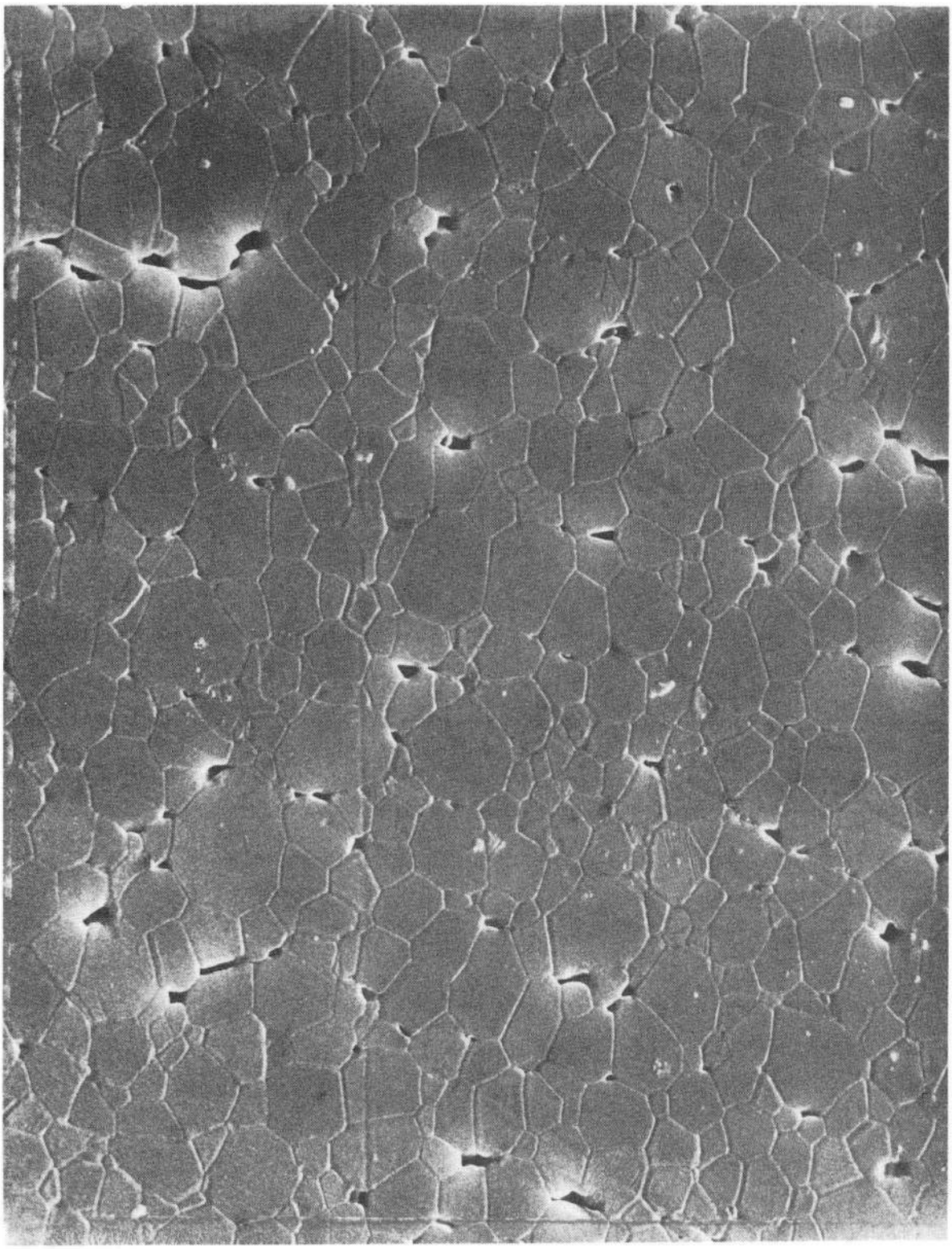

Fig. 9

XBB804-4499

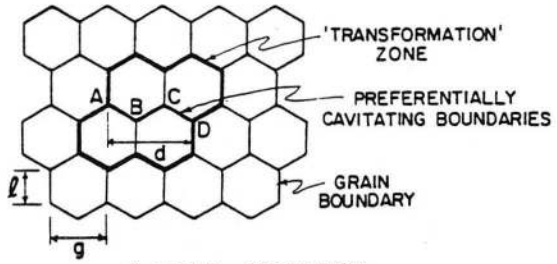

a) INITIAL CONDITION

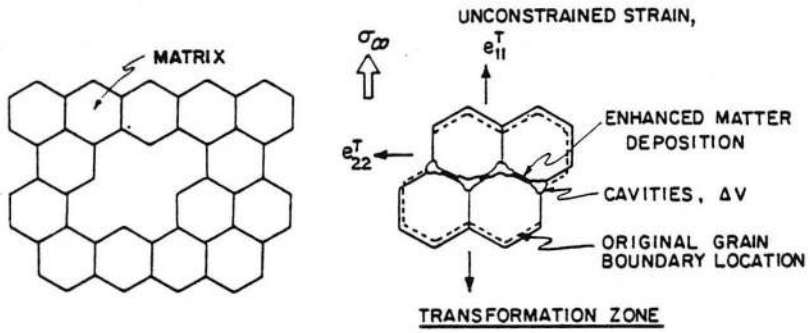

b) UNCONSTRAINED STRAIN

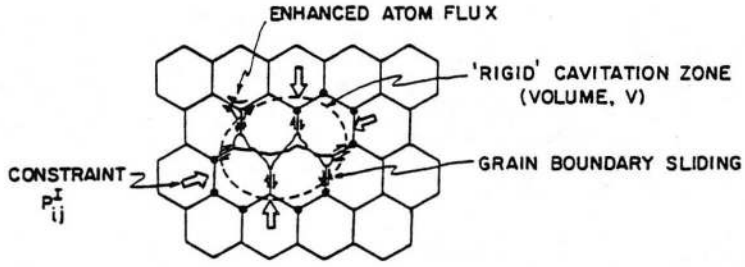

c) CONSTRAINED STRAIN

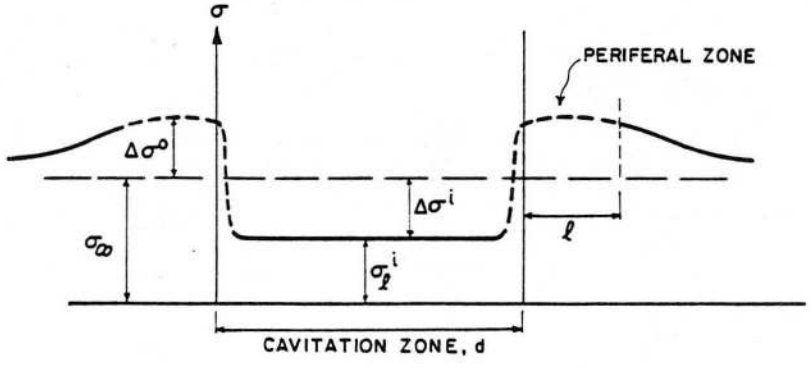

d) STRESS DISTRIBUTION

XBL813-5321

Fig. 10

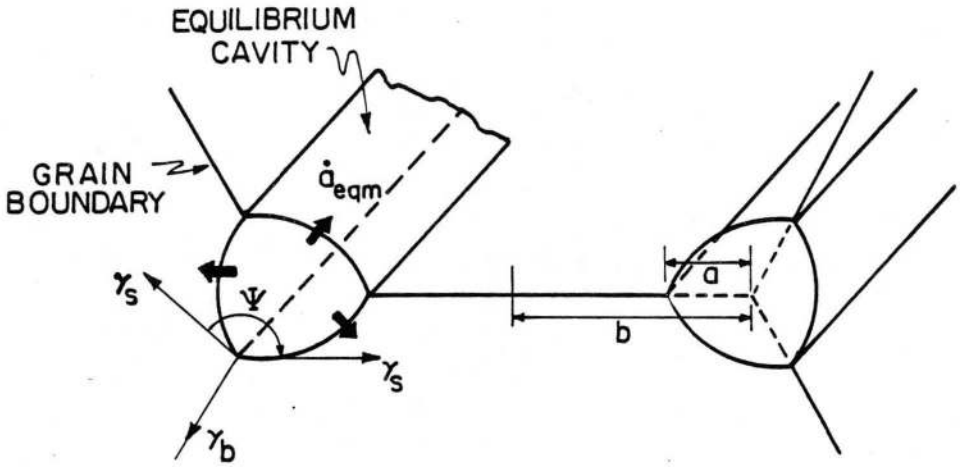

a) EQUILIBRIUM CAVITIES

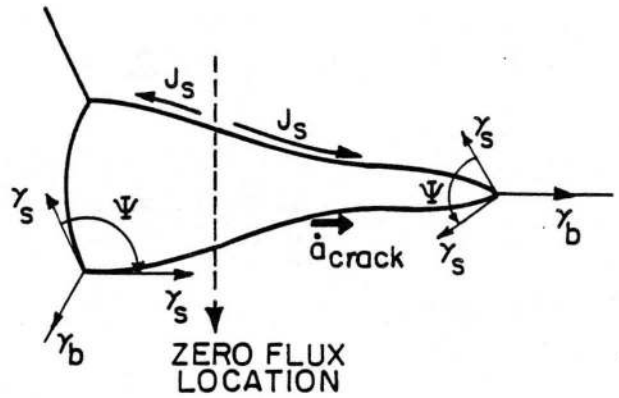

b) CRACK-LIKE CAVITY

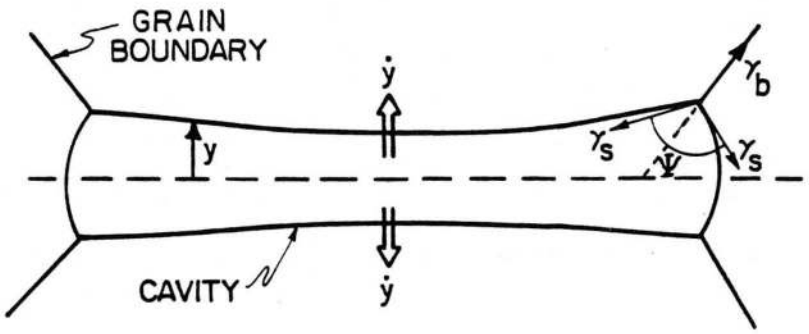

c) FULL-FACET CAVITY

XBL 816-6004

Fig. 11

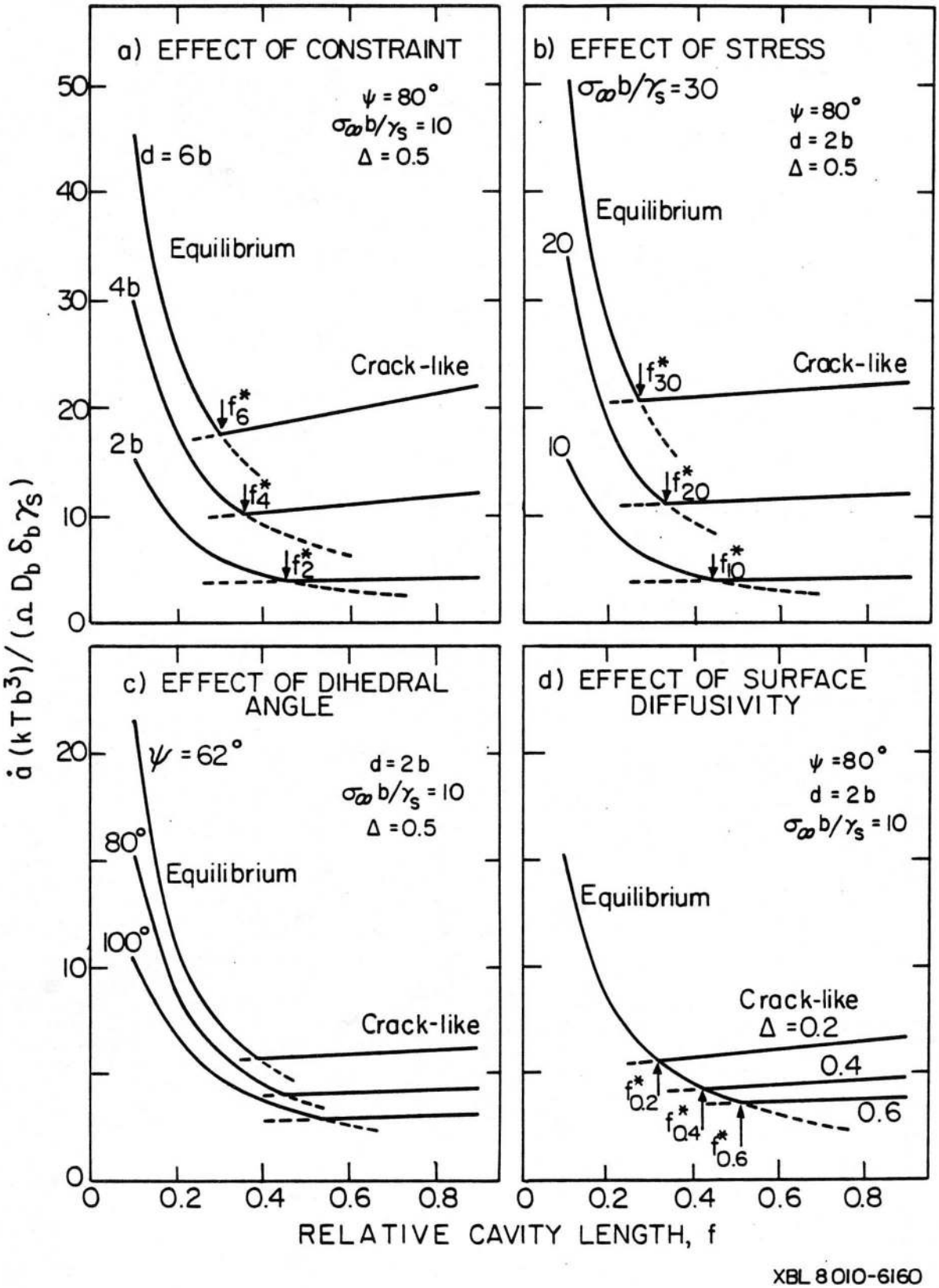

XBL 8010-6160

Fig. 12

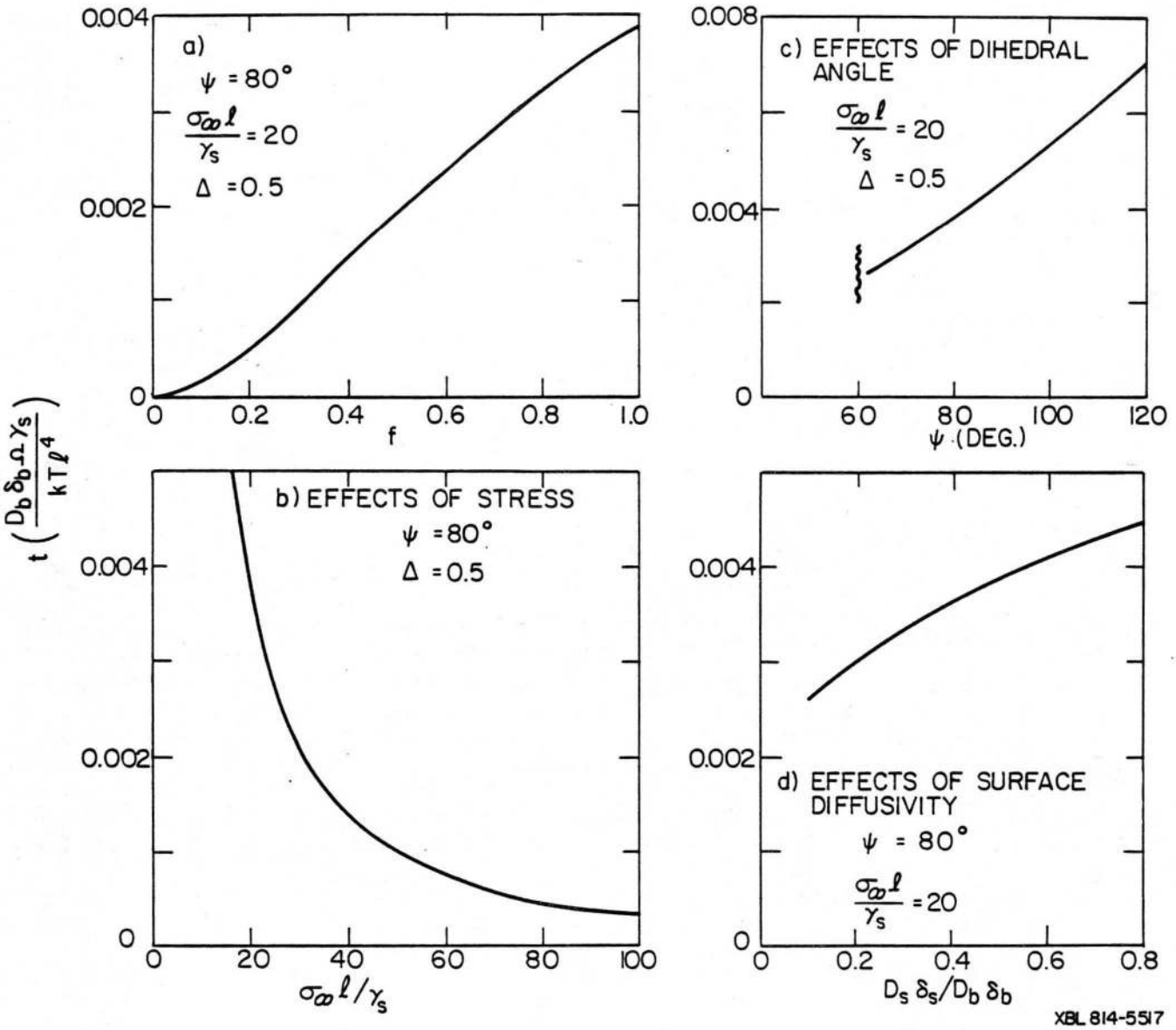
a)
ψ = 80°
σ∞ℓ/γs = 20
Δ = 0.5
f
c) EFFECTS OF DIHEDRAL ANGLE
σ∞ℓ/γs = 20
Δ = 0.5
ψ (DEG.)
b) EFFECTS OF STRESS
ψ = 80°
Δ = 0.5
σ∞ℓ/γs
d) EFFECTS OF SURFACE DIFFUSIVITY
ψ = 80°
σ∞ℓ/γs = 20
Ds δs/Db δb
t(Db δb Ω γs / kT ℓ⁴)
XBL 814-5517

Fig. 13

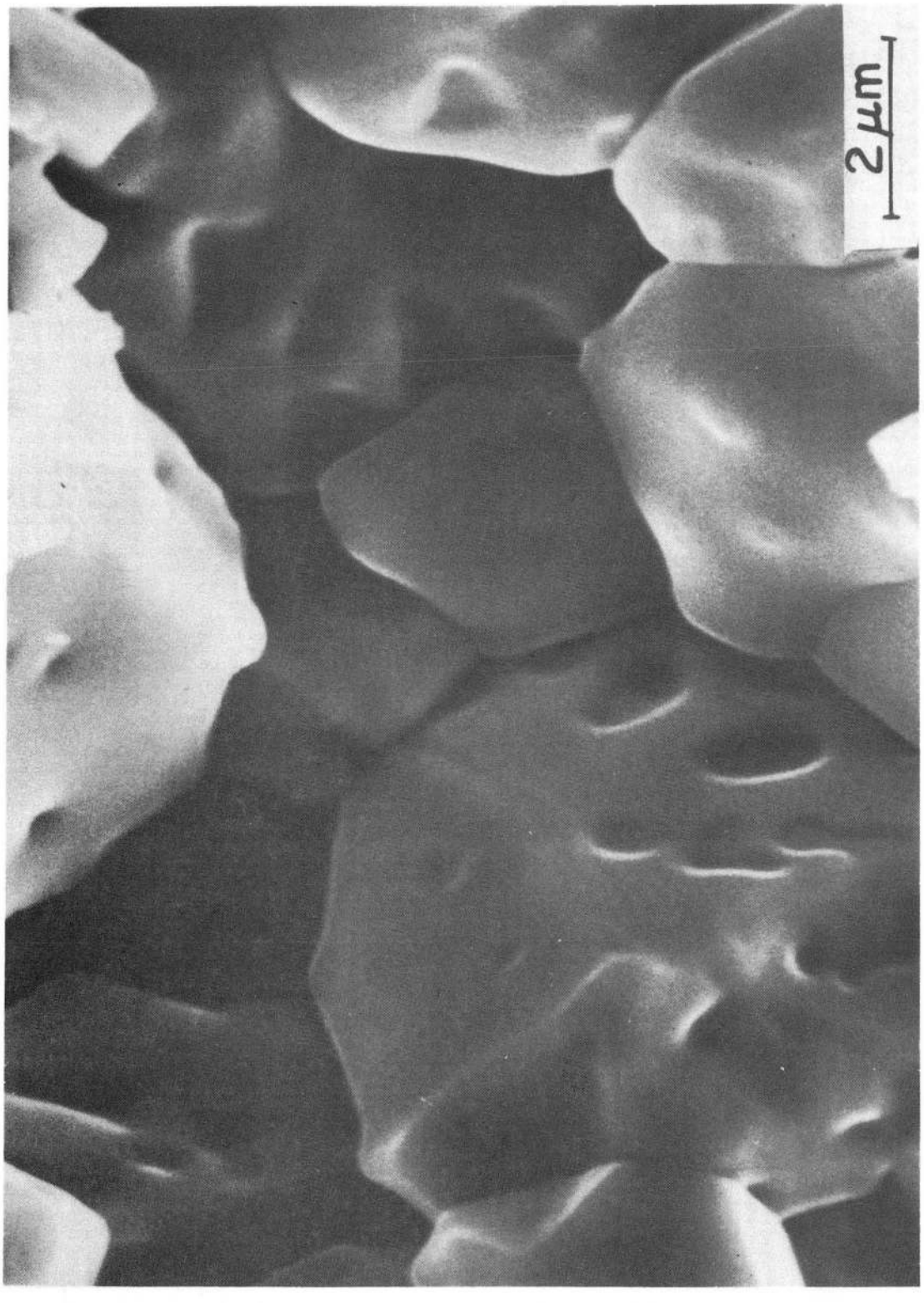

XBB813-2548

Fig. 14

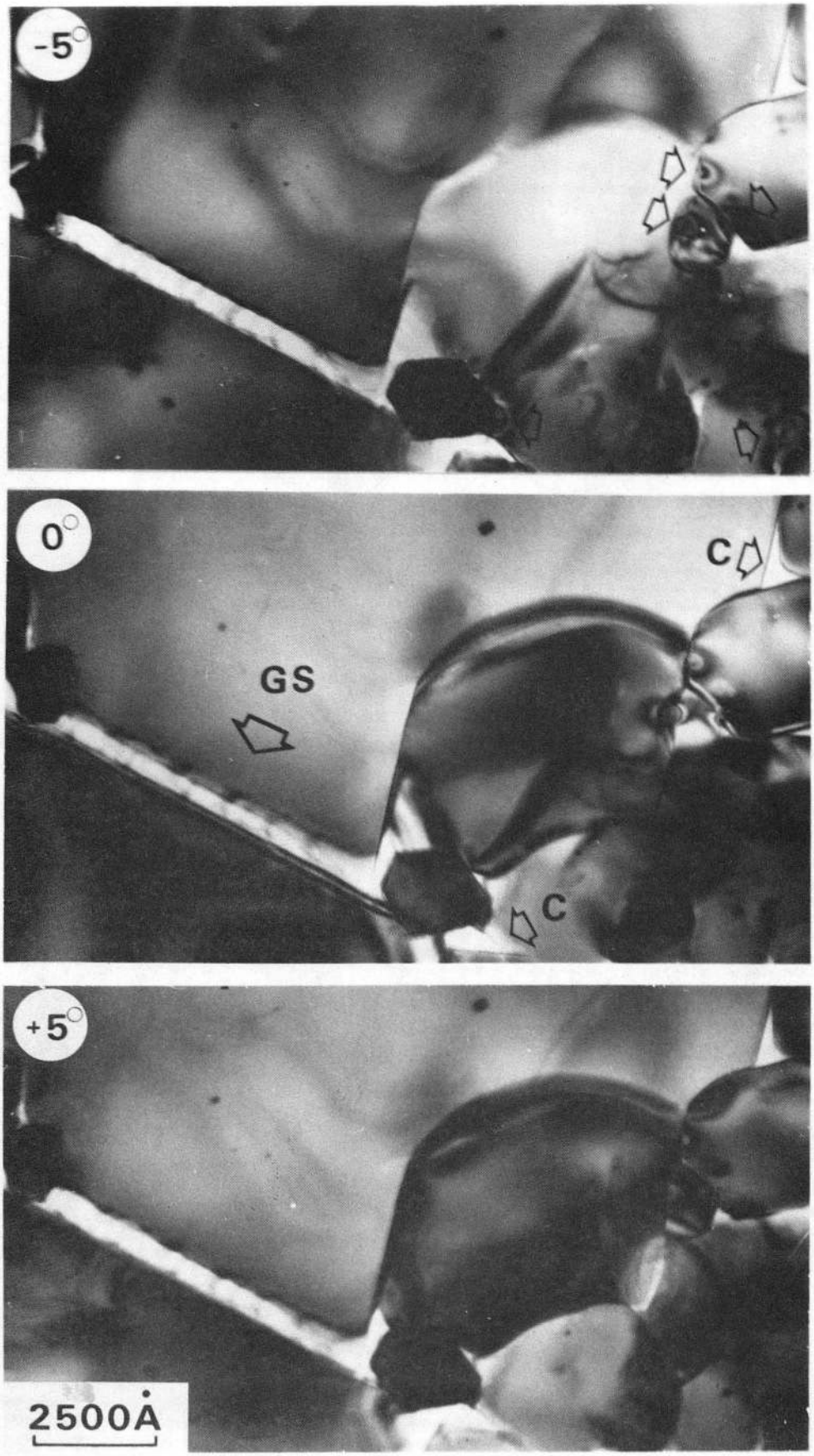

XBB813-2542

Fig. 15

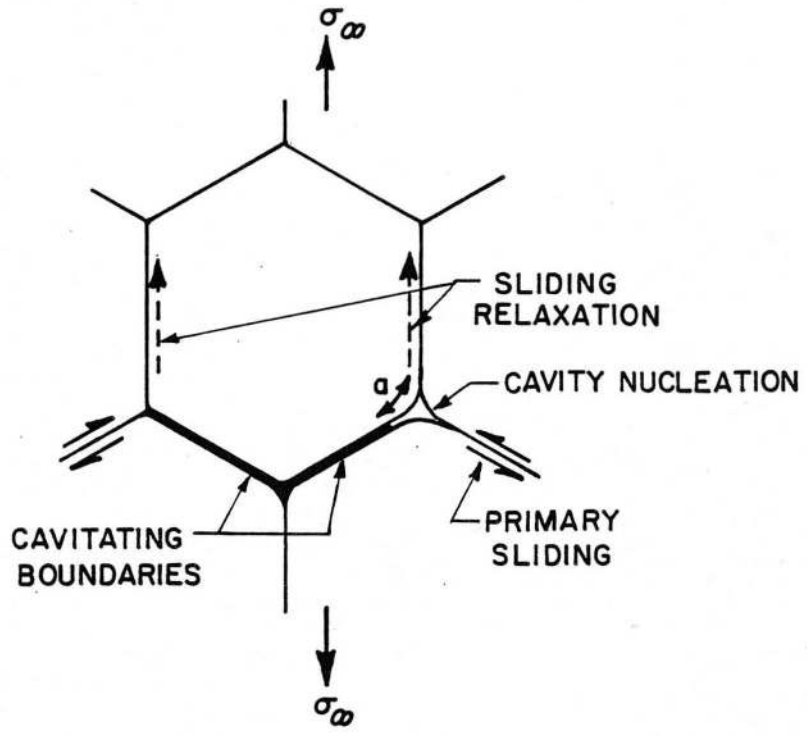

(a) NUCLEATION

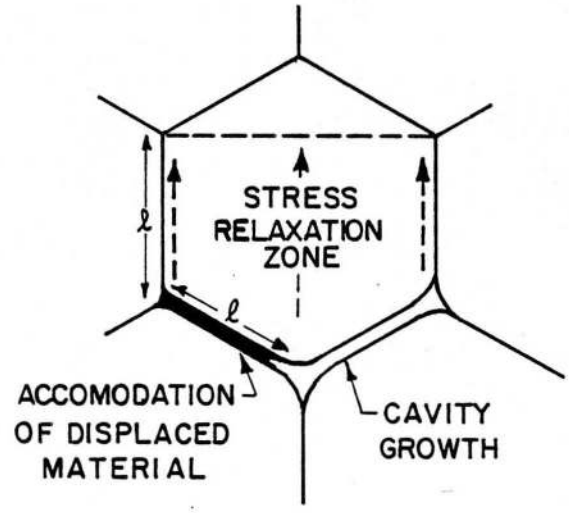

(b) EVOLUTION

XBL 793-5998

Fig. 16

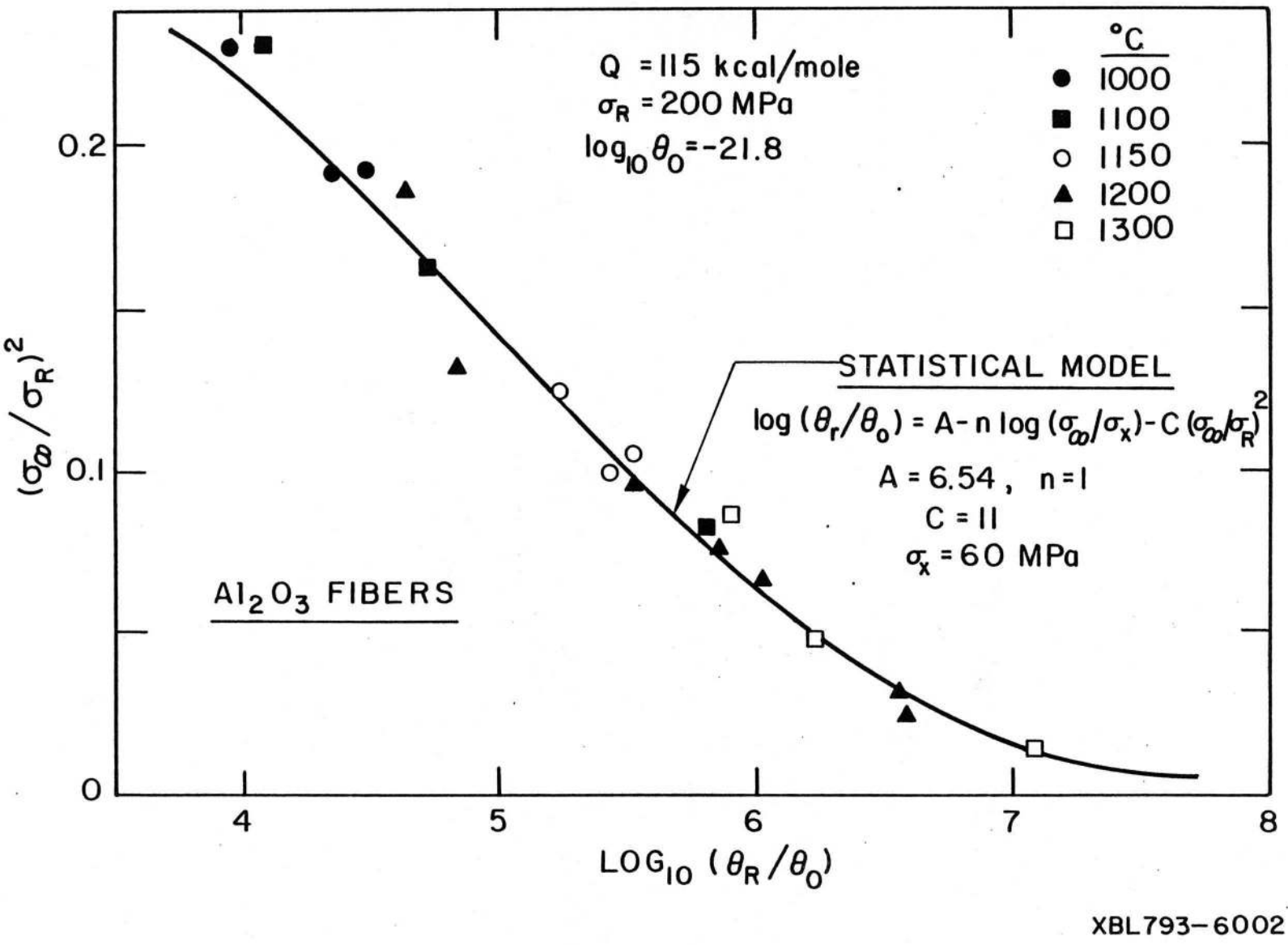

XBL793-6002

Fig. 17a

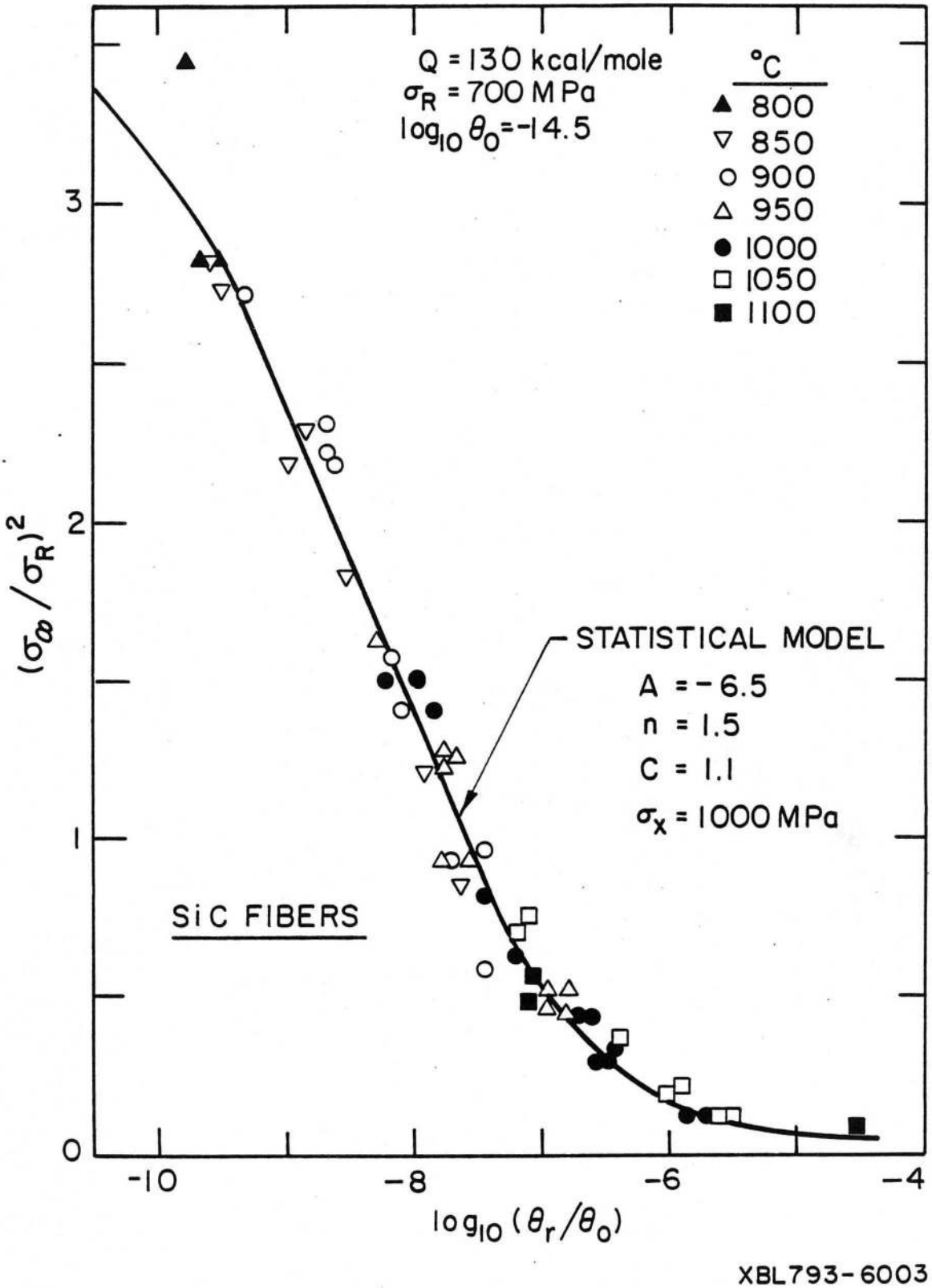
Q = 130 kcal/mole
σ_R = 700 MPa
$\log_{10}\theta_0$=-14.5
°C
800
850
900
950
1000
1050
1100
STATISTICAL MODEL
A = -6.5
n = 1.5
C = 1.1
σ_x = 1000 MPa
SiC FIBERS
$(\sigma_\infty/\sigma_R)^2$
$\log_{10}(\theta_r/\theta_0)$
0
1
2
3
-10
-8
-6
-4
XBL793-6003

Fig. 17b

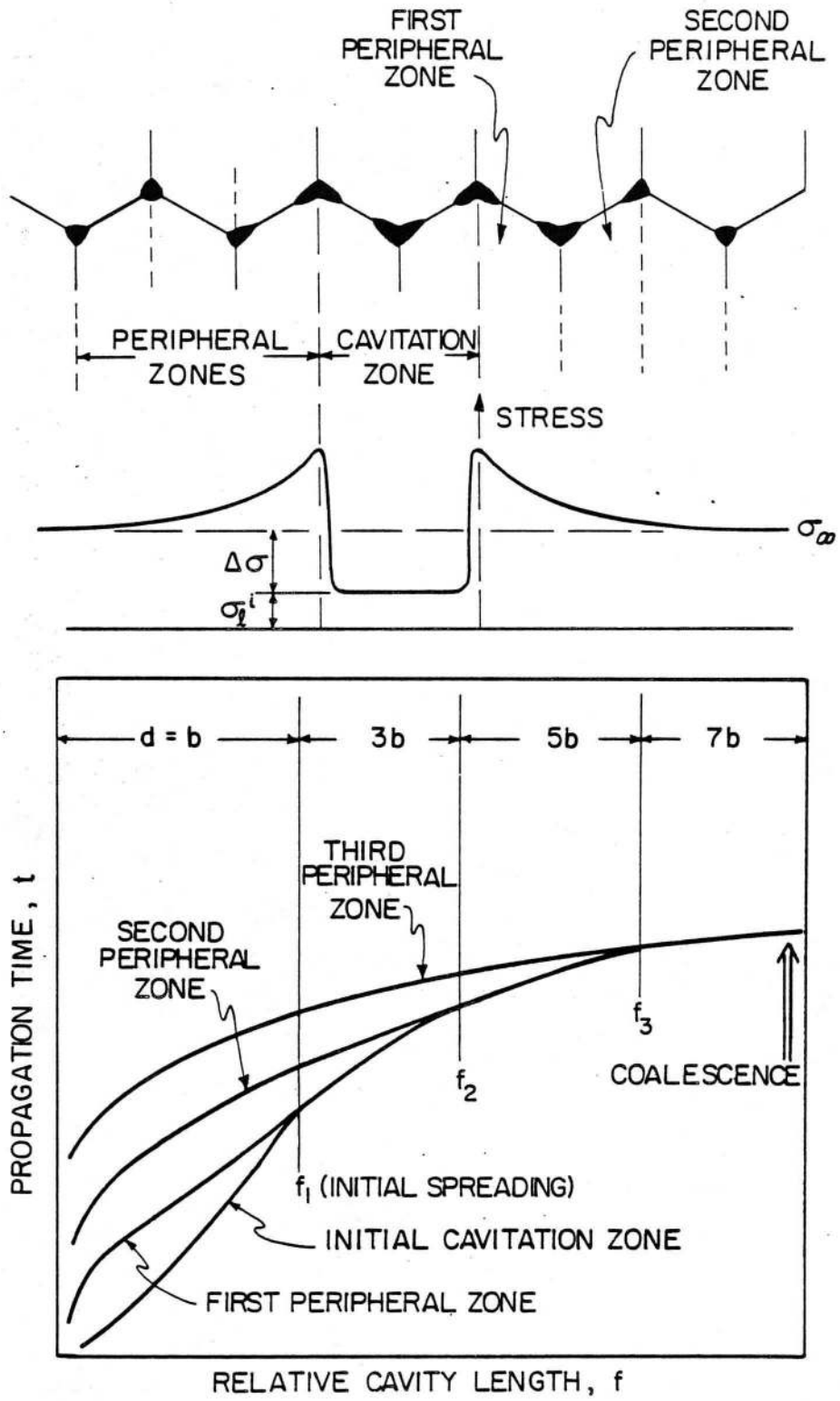
FIRST PERIPHERAL ZONE
SECOND PERIPHERAL ZONE
PERIPHERAL ZONES
CAVITATION ZONE
STRESS
σ_∞
$\Delta\sigma$
σ_i
d = b
3b
5b
7b
THIRD PERIPHERAL ZONE
SECOND PERIPHERAL ZONE
f_3
f_2
COALESCENCE
f_1 (INITIAL SPREADING)
INITIAL CAVITATION ZONE
FIRST PERIPHERAL ZONE
PROPAGATION TIME, t
RELATIVE CAVITY LENGTH, f
XBL 816-6005

Fig. 18

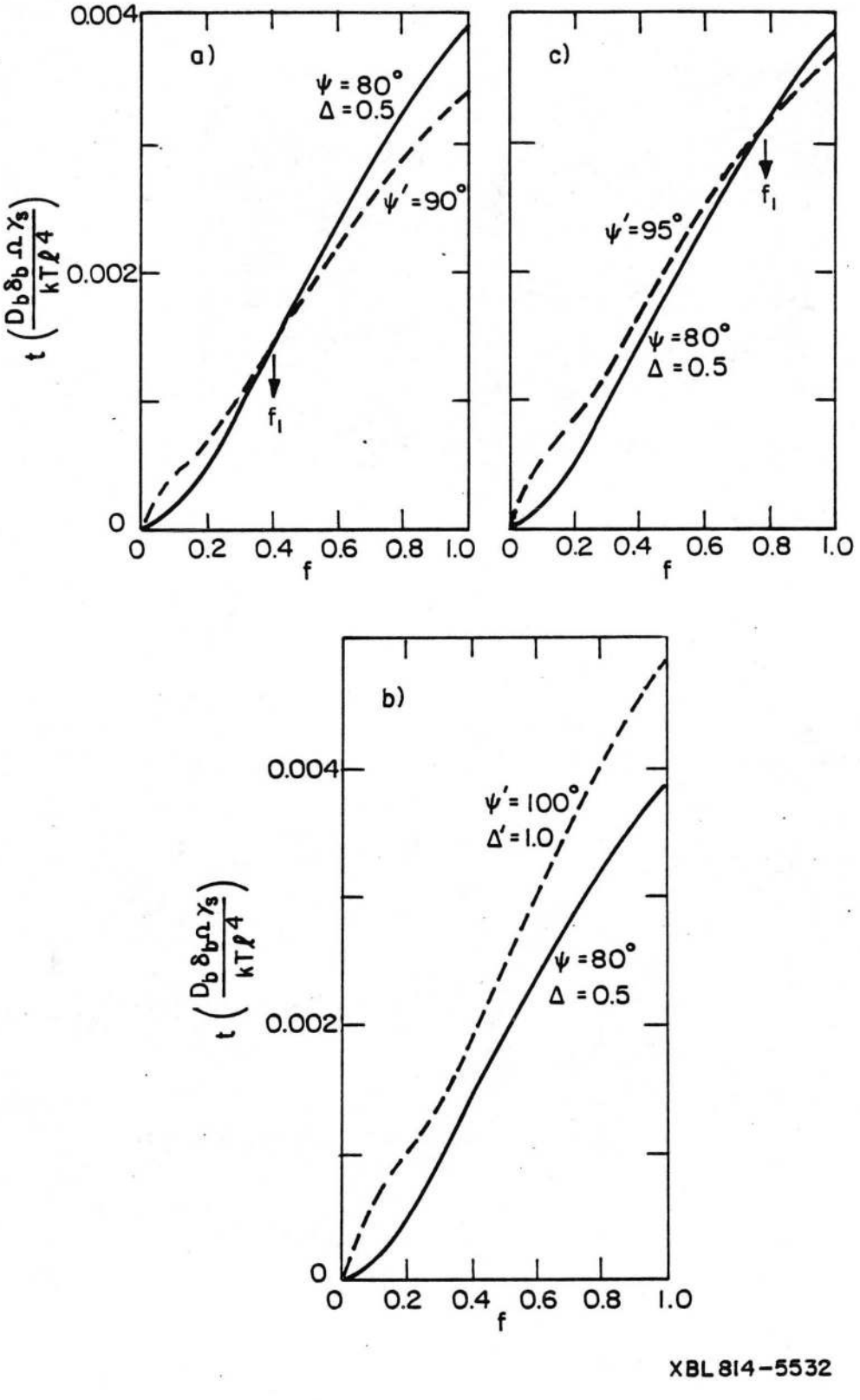
a)
ψ = 80°
Δ = 0.5
ψ' = 90°
f1
c)
ψ' = 95°
ψ = 80°
Δ = 0.5
f1
b)
ψ' = 100°
Δ' = 1.0
ψ = 80°
Δ = 0.5
0.004
0.002
0
0 0.2 0.4 0.6 0.8 1.0
f
t (Db δb Ω γs / kT ℓ4)
XBL 814-5532

Fig. 19

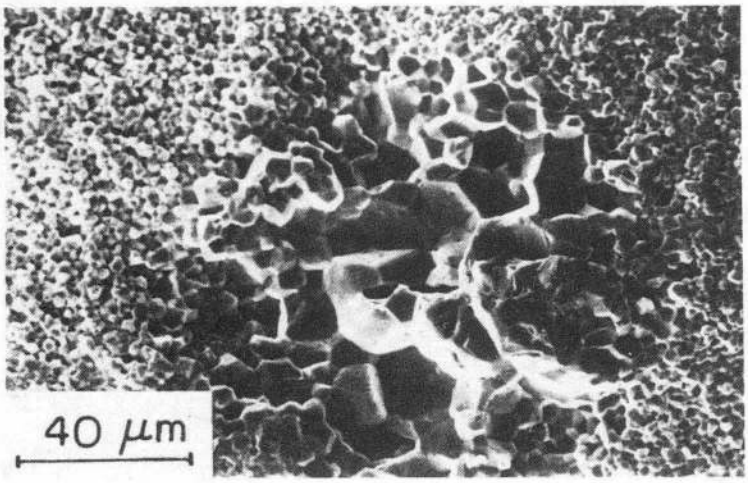

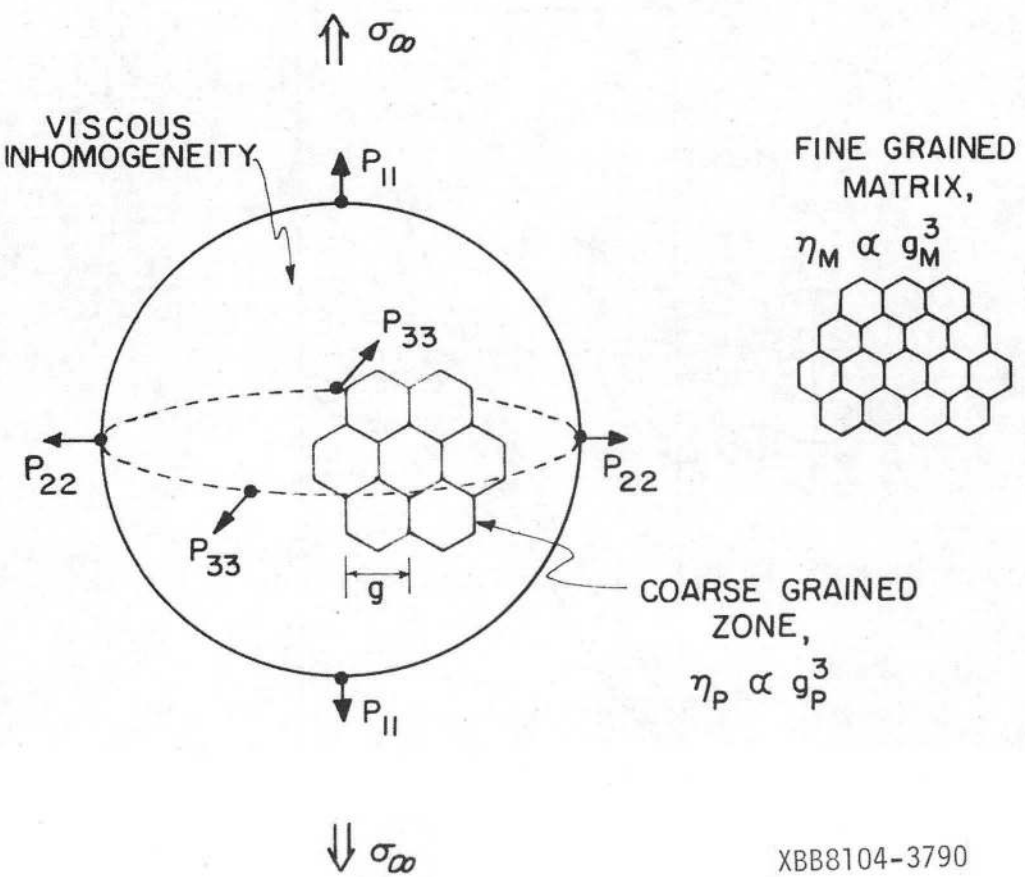

XBB8104-3790

Fig. 20

TECHNICAL INFORMATION DEPARTMENT
LAWRENCE BERKELEY LABORATORY
UNIVERSITY OF CALIFORNIA
BERKELEY, CALIFORNIA 94720